View metadata, citation and similar papers at core.ac.uk

brought to you by CORE

provided by Archive Ouverte en Sciences de l'Information et de la Communication

A hierarchy of models for the design of composite pressure vessels

Federica Daghia, E. Baranger, Duy Tien Tran, Pierre Pichon

▶ **To cite this version:**

Federica Daghia, E. Baranger, Duy Tien Tran, Pierre Pichon. A hierarchy of models for the design of composite pressure vessels. Composite Structures, Elsevier, In press. hal-02395907

HAL Id: hal-02395907

https://hal.archives-ouvertes.fr/hal-02395907

Submitted on 10 Dec 2019

HAL is a multi-disciplinary open access archive for the deposit and dissemination of scientific research documents, whether they are published or not. The documents may come from teaching and research institutions in France or abroad, or from public or private research centers.

L'archive ouverte pluridisciplinaire **HAL**, est destinée au dépôt et à la diffusion de documents scientifiques de niveau recherche, publiés ou non, émanant des établissements d'enseignement et de recherche français ou étrangers, des laboratoires publics ou privés.

A hierarchy of models for the design of composite pressure vessels

F. Daghia[a,*], E. Baranger[a], D.-T. Tran[a], P. Pichon[b]

[a] *LMT (ENS Paris-Saclay, CNRS, Univ. Paris-Saclay)*
61 av. du Président Wilson, F-94235 Cachan CEDEX, France
[b] *CETIM, Technocampus Composites*
Chemin du Chaffault, 44340 Bouguenais, France

Abstract

The mechanical response of pressure vessels to an applied internal pressure is essentially controlled by a few key parameters, related both to the overall geometry of the structure and to the orientations and thicknesses of the composite layers. The role of each parameter, and the way they interact to determine the structural response, can be apprehended at a very early design stage by using simple material and structural models, which enable to explore a wide range of designs with minimal computational cost. More complex models can then be called into play to predict the detailed structural response, including crucial information such as the burst pressure and failure mode. This paper discusses a hierarchy of models with increasing levels of details and complexity, which are useful to gain increasing insight on the pressure vessel response all along the design process.

Keywords: pressure vessels, filament winding, netting analysis, shell models

1. Introduction

In recent years, the use of continuous fiber, polymer matrix composites for the development of stiff and strong, but lightweight, structures has increased in multiple industrial domains. Commercially available pressure vessels, in particular, can be classified according to their composite content into four types:

- type I vessels are purely metallic;
- type II vessels have a metallic structure, reinforced with circumferential composite layers in their central portion [1];
- type III vessels have a metallic liner, reinforced with composite layers over their entire body [2];

*Corresponding author. Tel. +33 (0)1 47 40 28 31, Fax +33 (0)1 47 40 27 85.
Email address: federica.daghia@ens-paris-saclay.fr (F. Daghia)

- type IV vessels have a plastic liner, and their load bearing structure is entirely made of composite layers [3].

Type V vessels, which do not include a liner, are currently at the research stage [4]. Type IV pressure vessels are particularly interesting for the transportation industry, for example for the storage of high-pressure hydrogen in fuel cell vehicles [5, 6].

The mechanical response of type IV composite pressure vessels to an applied internal pressure is determined by two levels of geometrical features:

- the *external geometry*, that is the overall shape of the structure, usually composed of a cylindrical portion and two ends, or domes;
- the *internal geometry*, that is the orientation, thickness and sequence of the different composite layers (supposing that the liner bears no load).

All of these features, plus the choice of the composite material itself, constitute the design space within which the engineers can operate to define the final pressure vessel design. Making appropriate choices during the whole design process, and in particular in the preliminary design phase, is essential to obtain optimal structures, as well as to anticipate the presence of critical zones, which might require local reinforcements or other specific technical solutions.

In this work, we consider a hierarchy of material and structural models with increasing levels of details and complexity, which can be used sequentially from the preliminary to the final stages of structural design. While they are not necessarily very accurate, the simpler models are essential to enable the designer to understand and define the key geometric parameters, and in particular to analyze the interplay between the external and internal geometry in determining the mechanical response. The simplicity and extremely fast resolution of these models enables to rapidly explore many design possibilities at a very limited cost. Once the preliminary design has been defined, the more refined models enable the designer to predict in detail the mechanical response of the pressure vessel, accessing crucial information such as the burst pressure and failure mode.

Most of the models discussed in this work already exist in the literature, but they are revisited and/or extended here to be used within the overall design strategy of composite pressure vessels. In particular, the two steps strategy for the solution of a shell problem, based on the successive construction and solution of a membrane problem and a bending correction, is extended here to stacking sequences with a generally coupled membrane/bending behavior.

The bibliographic references related to the models discussed in the paper are given all along, where each of the models is presented. A glossary summarizing all of the used notations is reported in Appendix B.

2. Composite pressure vessel design space: external and internal geometries

2.1. External geometry

The overall shape of the pressure vessel is defined by the shape of the mandrel around which the composite layers are wound. An internal polymer layer, called liner, manufactured by rotational molding is used to ensure water tightness of the final structure, and the

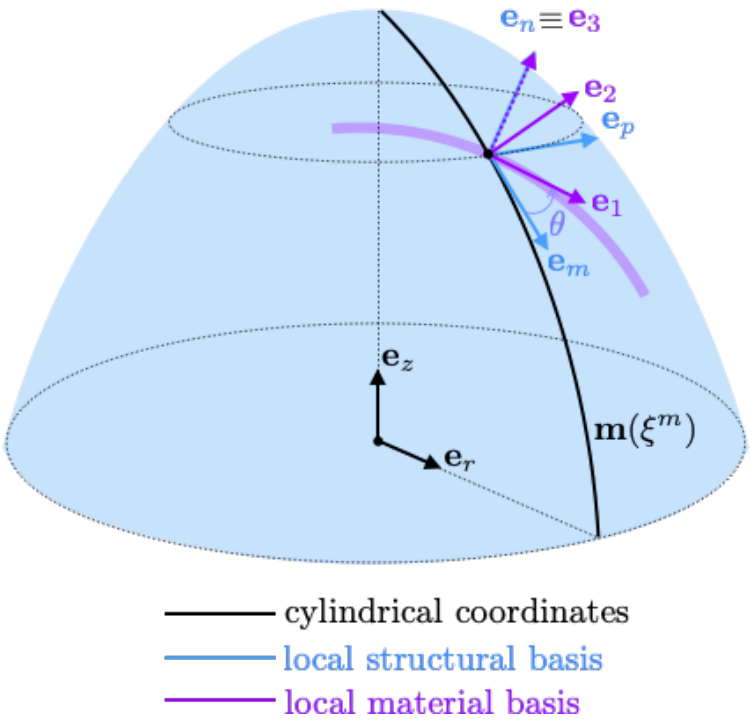

Figure 1: External and internal geometry of the pressure vessel and associated bases

composite layers are wound directly around the liner. The two ends of the pressure vessel are sealed by metal bases, which also serve as connections enabling to fill and to empty the pressure vessel. The number of deposed composite layers determine the thickness of the pressure vessel, thus it is defined here as part of the internal geometry (see Section 2.2).

In geometric terms, the shape of the pressure vessel can be described as a surface of revolution. Considering the cylindrical coordinates $(\mathbf{e}_r, \mathbf{e}_\theta, \mathbf{e}_z)$, the meridian curve $\mathbf{m}$, whose rotation around the $\mathbf{e}_z$ axis generates the surface, is defined as a parametric curve in the $(\mathbf{e}_r, \mathbf{e}_z)$ plane:

$$\mathbf{m}\left(\xi^m\right) = f_r\left(\xi^m\right)\mathbf{e}_r + f_z\left(\xi^m\right)\mathbf{e}_z \tag{1}$$

The definition the functions $f_r(\xi^m)$ and $f_z(\xi^m)$ for the chosen shape of the meridian curve is enough to completely define the geometrical properties of the resulting surface. In particular, at each position ξ^m along the meridian, one can define a local orthonormal basis for the structure $(\mathbf{e}_m, \mathbf{e}_p, \mathbf{e}_n)$ where $\mathbf{e}_m$ and $\mathbf{e}_p$ are the unit tangents to the meridian and the parallel, respectively, and $\mathbf{e}_n$ is the unit normal vector (see Figure 1). Furthermore, other useful quantities like the local metric tensor $\mathbf{g}$ and the local principal radii of curvature R_m and R_p can be computed. The specific expressions of these quantities as functions of f_r and f_z are reported in Appendix A.

In practice, the pressure vessel is often made up of two portions: a central cylindrical part of radius R and two heads, or domes, whose shape is dictated by mechanical as well

as practical considerations (such as the pressure vessel capacity with respect to its overall length). The geometry of the domes plays a major role in determining the internal stresses distribution in the domes themselves, as well as the magnitude of the local effects occurring at the junction between the domes and the central cylindrical portion of the vessel.

2.2. Internal geometry

The internal geometry is defined by the orientations, thicknesses and sequence of the composite layers.

In the following, the local orientation of each layer will be defined by the angle θ between the local vector $\mathbf{e}_m$ associated to the external geometry and the vector $\mathbf{e}_1$ defining the fibers' direction within the layer. The local basis for the material $(\mathbf{e}_1, \mathbf{e}_2, \mathbf{e}_3)$ is completed by defining the transverse in-plane direction $\mathbf{e}_2$ and the normal direction to the composite layer $\mathbf{e}_3 \equiv \mathbf{e}_n$ (see again Figure 1).

Axisymmetric structures such as pressure vessels are generally manufactured by filament winding. In this process, each composite layer is deposed by winding a fiber/matrix tow of a given width and thickness around the rotating mandrel. As a result, each layer generally includes tows oriented at both $+\theta$ and $-\theta$, with crossover patterns which depend on the winding parameters. To simplify matters, we neglect the effect of the crossover patterns in the following and we consider each layer as made up of tows at angles $\pm\theta$ in equal proportions.

Filament winding of thermoset matrix composites relies on some initial fibers' tension and on geodesic trajectories to keep the layers in place before curing of the polymer matrix, which occurs after winding. Small angles θ (lower than about 20°) are generally not accessible with this manufacturing process, and the evolution of the fibers' orientation along the surface of revolution is imposed by the geometry of the surface itself. Laser-assisted placement of thermoplastic matrix composite tape, on the other hand, is a more flexible process in which complex shapes and trajectories can be obtained, since the deposed tow is immediately welded to the previous layers by fast laser heating and subsequent cooling. Nevertheless, geodesic trajectories are still a popular choice for the manufacturing of thermoplastic-based pressure vessels, and they will be the only kind of trajectories considered here.

Geodesics on a surface of revolution obey Clairault's relation

$$f_r(\xi^m) \sin\left(\theta(\xi^m)\right) = \text{const} \tag{2}$$

which links the angle $\theta(\xi^m)$ between $\mathbf{e}_m$ and $\mathbf{e}_1$ to the distance $f_r(\xi^m)$ from the axis of revolution. As a consequence, the orientation of each layer is generally set to a certain constant value θ_0 in the cylindrical portion of the pressure vessel, while it evolves in the domes depending on their geometry. Furthermore, each layer can only be wound up to a minimum distance from the axis of revolution $f_{r,min}$, at which the fibers' direction becomes aligned with $\mathbf{e}_p$ (that is, $\theta(\xi^m) = 90°$):

$$f_{r,min} = R \sin\left(\theta_0\right) \tag{3}$$

where R is the radius of the cylindrical part of the pressure vessel. For a given thickness of the deposed tow, the local thickness of the composite layer also depends on $f_r(\xi^m)$, but this aspect will not be considered here.

This rapid description enables us to underline the complexity of the internal geometry of the pressure vessels, particularly in the domes. As it was discussed, the layers orientations and sequence are generally defined for the cylindrical part of the vessel, and their evolution as a function of the dome's geometry is endured but not really controlled by designers.

3. Material models

The two constituents, fibers and matrix, fulfill different roles in the overall mechanical response of the composite material. The fibers constitute the main load-bearing element and they control the stiffness and strength of the composite in the direction $\mathbf{e}_1$, while the matrix and the fiber/matrix interface enable the load transfer between fibers and control the transverse and interlaminar properties. Due to the symmetries associated to the fiber/matrix microstructure, the overall constitutive behavior of a composite tow is orthotropic in the material basis $(\mathbf{e}_1, \mathbf{e}_2, \mathbf{e}_3)$.

The different choices of the behavior of the composite tow are discussed in this Section. Based on the retained structural model, discussed in Section 4, the local behavior at the scale of the tow can be integrated to yield an overall shell-type behavior for the whole stacking sequence, or it can be used directly within a three-dimensional structural model.

Different descriptions of the constitutive behavior of the composite tow can be considered for different phases of the design process, with increasing level of complexity:

- if the stiffness and strength contributions of the fibers alone to the constitutive behavior is considered, the classical netting analysis is recovered [7, 8];
- if the contribution of both fibers and matrix is considered, but not their evolution related to progressive degradations, a full linear elastic orthotropic material model is defined: in the design phase, this elastic behavior is often completed with ply-level failure criteria (see for example the World Wide Failure Exercises [9, 10, 11]);
- if the progressive degradation of fibers, matrix and the fiber/matrix interface is considered, more complex models, such as continuum damage models, are introduced: different irreversible phenomena (microcracking, irreversible strain, ...) are accounted for in these models, thus enabling load redistribution during progressive degradation [12, 13].

The key aspects of each of the material models is discussed in the following.

3.1. Netting analysis

Although it is not always presented in classical references about the mechanics of composite materials, the netting analysis is a useful tool for preliminary design of composite pressure vessels.

The key hypothesis of this approach is that the fibers are the only load carrying element, thus completely neglecting the matrix contribution to the stiffness and strength of the composite. While this may seem an extreme simplification, it is indeed a sensible way to evaluate the pertinence and robustness of different choices of orientations and thicknesses to respond to specific sets of membrane loadings.

3.1.1. Classical presentation in terms of static quantities

The typical way to present netting analysis is in terms of static quantities only [7, 5]. As such, it may seem inappropriate to present this approach in the section about material models, but this apparent contradiction will be resolved later.

The plane stress state associated to each fiber orientation θ_i, written in the material coordinates $(\mathbf{e}_1, \mathbf{e}_2, \mathbf{e}_3)$ (subscript m), is assumed to have the following form:

$$\boldsymbol{\sigma}_i = \left[\begin{array}{ccc} \sigma_{11} & \sigma_{22} & \sigma_{12} \end{array} \right]^{\mathrm{T}} = \left[\begin{array}{ccc} \sigma_{11} & 0 & 0 \end{array} \right]^{\mathrm{T}}$$

Rotation of $\boldsymbol{\sigma}_i$ to the structural basis $(\mathbf{e}_m, \mathbf{e}_p, \mathbf{e}_n)$ and summation of the contributions from the different orientations yields the local equilibrium equations:

$$\sum_i \sigma_{11,i} t_i \left[\begin{array}{ccc} c_i^2 & s_i^2 & c_i s_i \end{array} \right]^{\mathrm{T}} = \left[\begin{array}{ccc} N_{mm} & N_{pp} & N_{mp} \end{array} \right]^{\mathrm{T}} \tag{4}$$

where, for each orientation θ_i, we have defined $c_i = \cos\theta_i$, $s_i = \sin\theta_i$ and the thickness t_i, while $\mathbf{N} = \left[\begin{array}{ccc} N_{mm} & N_{pp} & N_{mp} \end{array} \right]^{\mathrm{T}}$ are the membrane stresses associated to external loads.

This set of equations contains information only about the static part of the problem (local equilibrium), and so it may be over- or under-determined to compute the local stresses in the fibers for a given set of external loading, orientations and thicknesses. Its most common use is as a simple optimal design tool, to determine stacking sequences or choice of thicknesses in which the fibers in every direction are all equally loaded.

A classical example of the use of netting analysis is to determine the "optimal" winding angle $\theta = 54.74°$ for a cylinder with end closures under internal pressure, which is widely quoted but not always properly used in the literature. This result is obtained from Eq. (4) by assuming two winding angles $\theta_{1,2} = \pm\theta$ and a membrane biaxial stress state of the form (to be justified in Section 5)

$$\left[\begin{array}{ccc} N_{mm} & N_{pp} & N_{mp} \end{array} \right]^{\mathrm{T}} = \frac{pR}{2} \left[\begin{array}{ccc} 1 & 2 & 0 \end{array} \right]^{\mathrm{T}} \tag{5}$$

with p the internal pressure and R the radius of the cylinder. It should be noted that this is not the only optimal set of orientations and thicknesses, and that, as it will be seen in the following, it is not robust with respect to deviations from the ideal loading conditions considered.

3.1.2. Presentation in terms of simplified constitutive behavior

An alternative and very useful way to present the netting analysis in terms of simplified elastic behavior of the layer was introduced in [8].

There, the plane stress constitutive behavior of each fiber orientation θ_i in the material (layer) coordinates is written as

$$\boldsymbol{\sigma}_i = \mathbf{C}\boldsymbol{\varepsilon}_i \quad \Rightarrow \quad \left[\begin{array}{c} \sigma_{11} \\ \sigma_{22} \\ \sigma_{12} \end{array} \right]_i = \left[\begin{array}{ccc} E_1 & 0 & 0 \\ 0 & 0 & 0 \\ 0 & 0 & 0 \end{array} \right] \left[\begin{array}{c} \varepsilon_{11} \\ \varepsilon_{22} \\ 2\varepsilon_{12} \end{array} \right]_i$$

The layer stiffness matrix $\mathbf{C}$ has rank 1, thus the compliance is infinite in all directions except $\mathbf{e}_1$. In other words, a single orientation has no stiffness to support loads which are not aligned with the fibers' direction. Supposing that the membrane strains $\boldsymbol{\mu} = \begin{bmatrix} \mu_{mm} & \mu_{pp} & 2\mu_{mp} \end{bmatrix}^{\mathrm{T}}$ are constant in each layer, the membrane constitutive behavior for the whole stack in the structural basis can be defined as follows

$$\mathbf{N} = \mathbf{A}\boldsymbol{\mu}$$

where

$$\mathbf{A} = \sum_i t_i \mathbf{T}_i^{\mathrm{T}} \mathbf{C} \mathbf{T}_i$$

and the rotation operator $\mathbf{T}_i$ is defined as

$$\mathbf{T}_i = \begin{bmatrix} c_i^2 & s_i^2 & c_i s_i \\ s_i^2 & c_i^2 & -c_i s_i \\ -2c_i s_i & 2c_i s_i & c_i^2 - s_i^2 \end{bmatrix}$$

It should be noted that, from a physical point of view, it is the load transfer ensured by the matrix which justifies the hypothesis of constant membrane strains used to determine the behavior of the whole stack. Thus, while the matrix contribution to the stiffness of a tow is neglected, its load transfer role still needs to be assured if the composite is to behave as a structural assembly.

The membrane stiffness matrix $\mathbf{A}$ is rich of information. When only one or two fiber orientations are included in the stack, $\mathbf{A}$ is not a full rank matrix. The image of $\mathbf{A}$, which defines the set of membrane stresses which can be sustained by the structure, has dimension equal to the rank and it does not include the whole space of possible membrane stresses. For this reason, stacks including only one or two orientations are not robust to deviations from the ideal loading conditions the structure was designed for, as accidental loadings might end up being supported by the matrix only. Starting from three fibers orientations, $\mathbf{A}$ becomes a full rank matrix and any loading condition can be supported with at least a partial contribution from the fibers. This is the basis for the design recommendation to include at least four distinct fiber directions, with at least 10% fibers in each direction [7].

Using the whole stack behavior, the layer behavior and the rotation operator, the stress $\boldsymbol{\sigma}_i$ of layer i in the material (layer) basis can be linked to the membrane stresses $\mathbf{N}$ as

$$\boldsymbol{\sigma}_i = \mathbf{C}\boldsymbol{\varepsilon}_i = \mathbf{C}\mathbf{T}_i\boldsymbol{\mu} = \mathbf{C}\mathbf{T}_i \mathrm{inv}\left(\mathbf{A}\right)\mathbf{N} \tag{6}$$

where $\mathrm{inv}\left(\mathbf{A}\right)$ is the Moore-Penrose pseudoinverse (since $\mathbf{A}$ can be singular). Differently from the classical formulation based solely on static quantities, this expression enables one to quantify the fiber stresses for any number of different layer orientations.

Optimal design conditions based on the same ingredients discussed here (namely, a simplified constitutive behavior and the local equilibrium) were derived in [14]. In particular, it is shown that an infinity of optimal solutions exist, having the same total thickness t and

different combinations of orientations and relative thicknesses (θ_i, t_i). Furthermore, for cases with three or more different orientations, the optimal solution yields average strains which are invariant with respect to rotation (that is, $\boldsymbol{\mu} = \mu \begin{bmatrix} 1 & 1 & 0 \end{bmatrix}^{\mathrm{T}}$).

Let us consider for example the biaxial membrane stresses discussed previously (Eq. (5)). In addition to the famous solution $\theta = 54.74°$, a family of solutions of the form $(\pm\theta_1, \pm\theta_2, ..., \pm\theta_n)$ with $n \geq 2$ can be recovered, whose thicknesses can be determined by the equilibrium condition Eq. (4). A simple example is the set of orientations $(90°, \pm 45°)$, where each orientation has the same thickness. For $n > 2$, different combinations of thicknesses are possible to yield different optimal solutions for the same set of orientations. As discussed previously, the solutions having three or more fibers orientations are more robust with respect to accidental loadings when compared to the famous optimal solution with only two winding angles $\pm\theta$.

3.2. Full linear elastic behavior (and failure criteria)

The most classical way to describe the behavior of a composite tow is in terms of a linear elastic orthotropic solid, whose three-dimensional compliance matrix in the material coordinates reads

$$\mathrm{inv}\,(\mathbf{C}) = \begin{bmatrix} \frac{1}{E_1} & -\frac{\nu_{21}}{E_2} & -\frac{\nu_{31}}{E_3} & 0 & 0 & 0 \\ -\frac{\nu_{12}}{E_1} & \frac{1}{E_2} & -\frac{\nu_{32}}{E_3} & 0 & 0 & 0 \\ -\frac{\nu_{13}}{E_1} & -\frac{\nu_{23}}{E_2} & \frac{1}{E_3} & 0 & 0 & 0 \\ 0 & 0 & 0 & \frac{1}{G_{23}} & 0 & 0 \\ 0 & 0 & 0 & 0 & \frac{1}{G_{13}} & 0 \\ 0 & 0 & 0 & 0 & 0 & \frac{1}{G_{12}} \end{bmatrix} \tag{7}$$

The nine independent parameters (three Young's moduli E_i, three shear moduli G_{ij} and three of the six Poisson's coefficients ν_{ij}) result from the homogenized behavior of the fiber/matrix material. For an undamaged unidirectional tow, the behavior can be further simplified to transversely isotropic in the $(\mathbf{e}_2, \mathbf{e}_3)$ plane, thus resulting in five independent parameters.

Considering the matrix contribution to the stiffness, the compliance and stiffness matrices associated to a single orientation are full rank matrices, thus a single orientation can withstand any type of loading. Both stiffness and strength of a single tow, however, decline quickly when moving away from direction $\mathbf{e}_1$, thus a combination of at least three orientations is still good practice in order to respond more effectively to any loading conditions. In this sense, the extreme simplification associated to the netting analysis is useful to rapidly detect potential issues in the choice of the fiber orientations.

The full elastic behavior of a tow can be used directly within a three-dimensional computation, or it can be simplified to its plane stress version and combined with laminated theories in order to obtain the constitutive behavior of the shell. This enables one to investigate the response of the structure to any kind of loading conditions, and not only to membrane loadings as it was the case with the netting analysis.

The linear elastic analysis is usually complemented with one or more failure criteria associated to each fiber orientation, which are computed during post-processing to evaluate

the structural conditions with respect to some admissible values. A variety of criteria exist (see for example [9, 10, 11]), which can be based on specific failure mechanisms (fiber failure, matrix cracking, ...) or defined as an overall failure envelope which does not enable a clear distinction of the phenomena at play.

Composite materials are redundant by construction, and the possibility to share and, eventually, redistribute load is a key aspect of their mechanical behavior. As such, the fulfillment of one particular failure criteria may (or may not) be very conservative when evaluating the limit load. For instance, matrix cracking occurring along a single orientation hardly affects the overall behavior of the composite if the load can be redistributed to appropriately oriented fibers, while it may be catastrophic if (due to a design mistake) the matrix properties govern the composite behavior in some particular directions. Furthermore, failure criteria generally do not enable to clearly define the associated structural final failure mechanism, which can take a variety of forms: for pressure vessels, one may want to detect the creation of a communicating crack system which leads to leakage (as in [4]), or the bursting of the vessel with or without ejection of the metal base, ...

For all these reasons, elastic computations and failure criteria can be useful for preliminary design, but they are not enough to fully assess the response of the composite structure with respect to specific criteria in terms of burst pressure or failure mode.

3.3. Modeling the progressive degradation

A variety of approaches exist to account for progressive degradation and load redistribution in composite materials, from simple "last ply failure" approaches, which discard the stiffness associated to a given orientation when some criterion is fulfilled and recompute iteratively the solution until failure of the whole stack, to detailed micromechanical descriptions of matrix cracking, delamination and other degradations through fine-scale models such as [15]. For computations of a full structure, such as a pressure vessel, ply-scale continuum damage models appear as a reasonable compromise between accuracy of the description of the physical mechanisms and computational cost of the simulations. A variety of continuum damage models have been developed since the 1980s; in the following we discuss in particular the damage mesomodel developed at the LMT, in which the damage variables are constructed based on an underlying micromechanical description (see [12, 13] for a full description of the model and its validation in a number of test cases).

Starting from the orthotropic behavior of a healthy composite in the material basis Eq. (7), a set of internal variables and the associated evolution laws are introduced in the LMT damage mesomodel to describe the modification of the constitutive behavior as a function of the different physical degradation mechanisms within the ply. The degradation mechanisms within the ply which are accounted for include:

- fiber/matrix decohesion;
- transverse matrix cracking;
- fiber failure;

which modify the ply's stiffness in different directions, and eventually generate permanent deformation at unloading. Furthermore, an interface damage model (analogous to a cohesive zone model) is generally included in order to account for inter-ply delamination. A detailed identification procedure for the damage mesomodel parameters starting from standard tests on composite specimens was developed along with the model itself (see for example [16, 13]).

As it is the case for the full elastic behavior, the damage mesomodel can be used directly within three-dimensional simulations, or it can be reduced to a plane stress description and combined with laminate theories.

Due to the nonlinear material behavior, the overall response of the structure becomes nonlinear, thus generating more complex simulations than its linear elastic counterpart, including the need for multiple load steps, eventual convergence issues, localization and other potential numerical difficulties. In the general case, therefore, continuum damage models are best used in the last phases of the design process, when few potentially interesting designs need to be validated against some precise specifications (such as the requirement of a "safe" kind of burst failure mode, which does not eject the metal base). An example of damage based simulation of a type IV composite pressure vessel can be found in [6].

4. Structural models

The structural response of a pressure vessel to an applied internal pressure, and its eventual failure by leakage or burst, is one of the main aspects to be investigated during the design of these structures. As for the material description, different levels of complexity can be introduced for the structural description, enabling to gain different insights on the influence of the different design parameters (external and internal geometries) on the structural response.

The overall shape of a pressure vessel corresponds to a surface of revolution, with (relatively) small thickness with respect to the internal radius, thus shell models appear pertinent to describe the response of this type of structures in a (relatively) simple way.

Shell models were particularly popular in the 1960s for the design of homogeneous isotropic thin shells (see for example [17]). The complete shell model equations being too complex to solve analytically in the general case, a two-step solution strategy was developed, based on the successive construction of a main membrane solution, followed by a localized bending correction which re-establishes kinematic compatibility in the vicinity of critical points. This approach was the basis of shells design before the democratization of numerical simulation tools such as finite element analysis.

While membrane [18] and bending [19, 20] models were punctually applied to composite shell-like structures, to the authors' knowledge the two-step approach discussed in [17] for homogeneous shells has not been used for the preliminary design of composite shells. Although the many approximations involved lead to solutions which are potentially much less accurate than two-dimensional axisymmetric [21, 22, 23] or full three-dimensional computations, these simplified models can help the designer to acquire an understanding of the role played by the different design parameters on the overall structural response, and thus to make pertinent

design choices, ultimately decreasing the number of computationally expensive nonlinear simulations to be carried out to validate the final design.

4.1. Membrane model

Due to their small thickness, shell structures have relatively low bending stiffness, while their geometrical curvatures enable them to effectively respond to out-of-plane loadings with membrane stresses. For this reason, the simplest shell model can be obtained by neglecting the bending terms, yielding the so-called membrane model. Optimal shell design should aim for pure membrane loading, but, as we will see, this condition is quite hard to achieve in practice, due to punctual kinematic incompatibilities leading to localized bending effects.

4.1.1. Static analysis

In the membrane model of a general shell, the three unknown membrane stresses (two normal and one shear component) are related to each other by exactly three equilibrium equations (two associated to the in-plane directions and one to the out-of-plane direction). Depending on the boundary conditions, therefore, the problem can be solved purely by static analysis, without involving kinematic compatibility and material behavior. The independence of the internal stress state on the material behavior is particularly convenient, as any material description (from netting analysis to continuum damage models) can in principle be used simply as a post-processing of the membrane static analysis.

For the pressure vessel subjected to an internal pressure, the membrane stresses are described in the local shell basis $(\mathbf{e}_m, \mathbf{e}_p, \mathbf{e}_n)$ as:

$$\mathbf{N}(\xi^m) = \begin{bmatrix} N_{mm}(\xi^m) & N_{pp}(\xi^m) & 0 \end{bmatrix}^{\mathrm{T}}$$

where $N_{mm}(\xi^m)$ and $N_{pp}(\xi^m)$ are the membrane stresses in the meridian and parallel directions, respectively, and the membrane shear stress N_{mp} is zero due to axial symmetry of the (internal and external) geometry and the load.

The membrane stress in the meridian direction $N_{mm}(\xi^m)$ at each point of the shell can be determined by global equilibrium of the shell portion included between 0 and ξ^m. The resultant $\mathbf{Q}$ of the applied pressure $\mathbf{p} = p\,\mathbf{e}_n$ between 0 and ξ^m is computed as

$$\mathbf{Q}(\xi^m) = \int_0^{2\pi} \int_0^{\xi^m} p(\tau)\mathbf{e}_n \sqrt{g}\,\mathrm{d}\tau\mathrm{d}\theta = \left[2\pi \int_{f_r(0)}^{f_r(\xi^m)} p\left(f_r\right) f_r \mathrm{d}f_r\right] \mathbf{e}_z = Q_z(\xi^m)\mathbf{e}_z \qquad (8)$$

where g is the determinant of the metric tensor. Eq. (8) shows that the resultant $\mathbf{Q}$ is directed along $\mathbf{e}_z$, and that $Q_z(\xi^m)$ does not depend on the shape of the meridian surface, but only on the applied pressure $p(f_r)$ and on the radial coordinate f_r. In particular, for a shell which is closed at the top ($f_r(0) = 0$) with constant applied pressure ($p(f_r) = \bar{p}$), $Q_z(\xi^m)$ becomes

$$Q_z(\xi^m) = \bar{p}\pi f_r^2(\xi^m)$$

Global equilibrium of the shell portion then reads

$$Q_z + N_{mm}\,(2\pi f_r)\,\mathbf{e}_m \cdot \mathbf{e}_z = 0 \tag{9}$$

which enables one to determine N_{mm}.

Local equilibrium along $\mathbf{e}_n$, on the other hand, leads to the following equation

$$\frac{N_{mm}}{R_m} + \frac{N_{pp}}{R_p} + p = 0 \tag{10}$$

which highlights the role of the radii of curvature R_m and R_p in enabling the shell membrane response to out-of-plane loads. Since N_{mm} is already known from global equilibrium, this equation enables one to compute N_{pp}.

4.1.2. Kinematic description

As shown above, the membrane stresses within the shell can be determined simply by static analysis if the membrane model is considered. As such, the kinematic description can be invoked only *a posteriori*, to recover the strains and the displacements resulting in the membrane for a given loading condition. We will see here that the strains resulting from a purely membrane model cannot in the general case be integrated to yield a continuous displacement: that is where the need for a bending correction arises.

For the membrane model, and due to the symmetries of the problem, the shell displacement can be described by two scalar functions of ξ^m, the meridian displacement $u_m(\xi^m)$ and the normal displacement $u_n(\xi^m)$. We have:

$$\mathbf{u}(\xi^m) = u_m(\xi^m)\mathbf{e}_m + u_n(\xi^m)\mathbf{e}_n \tag{11}$$

It should be noticed that the rotation of the section has not been considered, as the bending terms are supposed to be negligible.

Starting from Eq. (11), the membrane strains $\boldsymbol{\mu}(\xi^m) = \left[\begin{array}{ccc} \mu_{mm}(\xi^m) & \mu_{pp}(\xi^m) & 0 \end{array}\right]^{\mathrm{T}}$ can be expressed as follows:

$$\begin{aligned} \mu_{mm} &= \frac{\sqrt{g_{mm}}}{g_{mm}}\left(u_m' - \Gamma^m_{mm} u_m\right) - \frac{u_n}{R_m} \\ \mu_{pp} &= \frac{\sqrt{g_{mm}}}{g_{pp}}\left(-\Gamma^m_{pp} u_m\right) - \frac{u_n}{R_p} \end{aligned} \tag{12}$$

where g_{ij} are the components of the metric tensor, Γ^i_{jk} are the Christoffel symbols, R_i are the radii of curvature and the superscript $'$ denotes the derivative with respect to the parameter ξ^m. The expressions of all of these terms as functions of the shape of the meridian curve are given in Appendix A. As it can be noticed, the presence of curvatures leads to coupling between the membrane strains and the out-of-plane displacement u_n, which is the kinematic dual of the local equilibrium equation Eq. (10) with respect to strain energy.

Since the membrane stresses have already been determined through static analysis, the membrane strains can be computed from the constitutive behavior as

$$\boldsymbol{\mu}(\xi^m) = \text{inv}\left(\mathbf{A}(\xi^m)\right)\mathbf{N}(\xi^m) \tag{13}$$

where the membrane stiffness matrix $\mathbf{A}$, obtained by integration of the composite's stiffness over the thickness, also depends on ξ^m since the orientation and number of plies is not generally the same at each point along the meridian curve (particularly in the dome). As it was pointed out before, any of the constitutive models discussed in Section 3 can be used to determine the matrix $\mathbf{A}$, yielding generally different results and, in the case of the netting analysis or of very significant damage evolution, a possibly singular $\mathbf{A}$. The strains computed from Eq. (13) can then be injected in Eq. (12).

Integration of Eq. (12) to obtain displacement functions $u_m(\xi^m)$ and $u_n(\xi^m)$ which are continuous over the whole domain is not always possible. Indeed, integration of the second line of Eq. (12) over the whole domain would require the membrane strain μ_{pp} to be continuous in ξ^m, but this is not guaranteed by the purely static solution. Discontinuities in the membrane strain μ_{pp} are generated by the external and/or the internal geometries:

- for the external geometry: a discontinuity of the meridian radius of curvature R_m (for example, at the junction between the cylinder and the dome) generates a discontinuous membrane stress N_{pp} via Eq. (10);
- for the internal geometry: a ply drop generates a discontinuous stiffness matrix $\mathbf{A}$.

A discontinuity of N_{pp} or $\mathbf{A}$ translates into a discontinuity of μ_{pp} via Eq. (13).

The lack of a continuous displacement solution for the general case highlights a limit of the purely membrane model. A two-step solution can nevertheless be devised, where the incompatibilities eventually identified by integrating the purely membrane model are resolved by introducing (localized) bending corrections to restore the continuity of displacements.

4.2. Bending correction

Restoring the compatibility of the displacements resulting from the membrane model requires the introduction of bending terms in the shell theory.

As it was stated earlier, the complete analytical solution of the whole shell model in the general case is complex even for homogeneous isotropic shells, let alone for the composite case. Luckily, the bending solution is localized in the vicinity of the disturbance, with a penetration length that decreases as the ratio of the membrane to bending stiffness increases, as it will be shown later in this Section. For this reason, a first estimation of the bending effects for any shell geometry can be obtained by considering the much simpler solution for a cylindrical shell, whose radius and (constant) stiffness are equal to those of the general shell in correspondence of the disturbance. This approximation was regularly used for the design of thin shells in the past [17] and its bounds were rigorously defined for homogeneous isotropic shells. Here, the aim is just to obtain a first estimate of the bending effects, and in particular to understand their sources and the key parameters at play, while the final

validation of the retained geometry will be performed using two-dimensional axisymmetric or full three-dimensional finite element simulation. As such, the accuracy of this approximation is less crucial here, and it will not be the focus of the discussion.

The equations for the cylindrical shell under bending loadings are derived in the following. With respect to the classical derivation, we consider here the more general case of unbalanced laminates, which introduces coupling terms between the membrane and bending constitutive behavior.

4.2.1. Model equations for a cylinder under bending loading

In the bending model, the equilibrium equations alone do not enable one to determine the static solution, thus the full model equations (kinematic, static and constitutive) need to be considered together.

The geometry of the cylinder is described here by the following parametrized meridian curve

$$\mathbf{m}(\xi^m) = R\mathbf{e}_r - R\xi^m\mathbf{e}_z, \quad \xi^m \geq 0$$

The rest of the geometrical quantities are derived according to the equations given in Appendix A.

The kinematic description needs to be enriched with respect to the membrane model, by including the section rotation and the associated bending strains. We have:

$$\mathbf{u}(\xi^m, \xi^n) = \left[u_m(\xi^m) + \xi^n\phi_m(\xi^m)\right]\mathbf{e}_m + u_n(\xi^m)\mathbf{e}_n \tag{14}$$

where ξ^n denotes the normal coordinate with respect to the shell midplane, and the rotation ϕ_m is related to the normal displacement according to the Kirchhoff-Love hypotheses, as $\phi_m = -u_n'/R$. The strains are expressed as

$$\text{membrane} \begin{cases} \mu_{mm} = \dfrac{u_m'}{R} \\ \mu_{pp} = \dfrac{u_n}{R} \end{cases} \qquad \text{bending} \begin{cases} \chi_{mm} = -\dfrac{u_n''}{R^2} \\ \chi_{pp} = 0 \end{cases}$$

where the membrane strains are identical to Eq. (12) specialized for the cylindrical geometry, while the bending strain χ_{mm} (change in curvature of the meridian) appears as an additional term.

The static description involves the following two equilibrium equations:

$$\begin{aligned} N_{mm}' &= 0 \\ \frac{M_{mm}''}{R^2} - \frac{N_{pp}}{R} + p &= 0 \end{aligned} \tag{15}$$

The first of Eqs. (15) immediately yields a constant meridian membrane stress N_{mm} in the cylinder, while the second one corresponds to Eq. (10), specialized for the cylinder and including also the bending contribution. Solving it requires to express M_{mm} and N_{pp} in terms of displacements, calling upon the constitutive and compatibility equations.

Considering a general stack of $\pm\theta$ layers, not necessarily balanced with respect to the shell midplane, we obtain the following constitutive behavior

$$\left[\begin{array}{c} \mathbf{N} \\ \mathbf{M} \end{array} \right] = \left[\begin{array}{cc} \mathbf{A} & \mathbf{B} \\ \mathbf{B}^{\mathrm{T}} & \mathbf{D} \end{array} \right] \left[\begin{array}{c} \boldsymbol{\mu} \\ \boldsymbol{\chi} \end{array} \right] \tag{16}$$

where $\mathbf{A}$ was previously defined and we have

$$\mathbf{B} = \sum_i \frac{\left(\xi_{i+1}^n\right)^2 - \left(\xi_i^n\right)^2}{2} \mathbf{T}_i^{\mathrm{T}} \mathbf{C}_i \mathbf{T}_i$$

$$\mathbf{D} = \sum_i \frac{\left(\xi_{i+1}^n\right)^3 - \left(\xi_i^n\right)^3}{3} \mathbf{T}_i^{\mathrm{T}} \mathbf{C}_i \mathbf{T}_i$$

where ξ_i^n and ξ_{i+1}^n are the positions of the bottom and the top of layer i. Due to the symmetries of the problem, the three constitutive matrices $\mathbf{A}$, $\mathbf{B}$ and $\mathbf{D}$ have the following structure

$$\bullet = \left[\begin{array}{ccc} \bullet_{11} & \bullet_{12} & 0 \\ \bullet_{12} & \bullet_{22} & 0 \\ 0 & 0 & \bullet_{33} \end{array} \right]$$

As for the matrix $\mathbf{A}$ already considered in the membrane model, the constitutive matrices $\mathbf{B}$ and $\mathbf{D}$ could, in principle, be determined using any of the material behaviors described in Section 3. The use of the simplified "netting analysis" behavior, however, is not recommended, as the contribution of each orientation also depends on its position relative to the midplane, thus making it not obvious to presuppose that certain stiffness terms can be neglected. Continuum damage models, on the other hand, lead to stiffness matrices which vary in both space and time, since the degradation evolves according to the local loading conditions: using this kind of material models significantly complexifies the problem, and would not lead to the simple closed-form solutions which are discussed in the following, and which enable one to understand the main parameters controlling the amplitude and penetration length associated to the bending problem. For this reason, the full linear elastic behavior for each ply appears as the wisest choice of material model in conjunction with the shell bending problem.

Since N_{mm} is constant and known from equilibrium, Eq. (16) can be used to express μ_{mm} as a function of N_{mm} and of the other strain components, which depend on the normal displacement u_n only. Substitution of the constitutive and compatibility equations into the section of Eq. (15) yields

$$\frac{\tilde{D}}{R^4} u_n'''' - \frac{2\tilde{B}}{R^3} u_n'' + \frac{\tilde{A}}{R^2} u_n = p - \frac{A_{12}}{A_{11}} \frac{N_{mm}}{R} \tag{17}$$

where the modified stiffness terms $\tilde{D}$, $\tilde{B}$ and $\tilde{A}$ are defined as

$$\tilde{D} = D_{11} - \frac{B_{11}^2}{A_{11}}, \quad \tilde{B} = B_{12} - \frac{B_{11} A_{12}}{A_{11}}, \quad \tilde{A} = A_{22} - \frac{A_{12}^2}{A_{11}}$$

The solution of this equilibrium equation is composed of two portions: the particular solution associated to the second member yields the constant u_n already determined in Section 4.1 through the membrane model, while the solution to the homogeneous equation recovers the bending terms.

The homogeneous equation can be put in the form

$$u_n'''' - \beta u_n'' + 4\alpha^4 u_n = 0 \tag{18}$$

where α and β are expressed as

$$\alpha = \left(\frac{R^2}{4} \frac{\tilde{A}}{\tilde{D}} \right)^{\frac{1}{4}}, \quad \beta = \frac{2\tilde{B}R}{\tilde{D}} \tag{19}$$

In particular, α is related to the ratio between the membrane and the bending stiffness, while β appears due to the coupling term $\tilde{B}$. The solution reads

$$u_n(\xi^m) = e^{-\alpha_1 \xi^m} \left[C_1 \sin(\alpha_2 \xi^m) + C_2 \cos(\alpha_2 \xi^m) \right] + e^{\alpha_1 \xi^m} \left[C_3 \sin(\alpha_2 \xi^m) + C_4 \cos(\alpha_2 \xi^m) \right] \tag{20}$$

where

$$\alpha_1 = \alpha\sqrt{2} \cos\left(\frac{\phi}{2}\right)$$

$$\alpha_2 = \alpha\sqrt{2} \sin\left(\frac{\phi}{2}\right)$$

$$\phi = \begin{cases} \arctan\left(\frac{\sqrt{16\alpha^4 - \beta^2}}{\beta} \right) & \text{if } \beta > 0 \\ \arctan\left(\frac{\sqrt{16\alpha^4 - \beta^2}}{\beta} \right) + \pi & \text{if } \beta < 0 \end{cases}$$

The four integration constants $C_1 - C_4$ can be determined for specific values of concentrated transverse shear forces Q_m^0 and moments M_{mm}^0 applied at $\xi^m = 0$. In particular, $C_1 = C_2 = 0$ in the shell portion with decreasing ξ^m, and $C_3 = C_4 = 0$ in the shell portion with increasing ξ^m, as the exponential term should decrease far from the disturbance.

The solution of the bending problem, Eq. (20), is well known for balanced laminates, and it was derived here for the more general case. Due to the real exponential term ($\pm\alpha_1 \xi^m$), it is localized in the vicinity of the disturbance, and its penetration length along the cylinder in the dimensionless coordinate ξ^m is proportional to $1/\alpha_1$. Setting $\tilde{B} = 0$, we recover the well-known result for the uncoupled case: $\phi = \pi/2$ and $\alpha_1 = \alpha_2 = \alpha$, thus the penetration length depends exclusively on the ratio of the membrane to bending stiffness.

4.2.2. Bending correction strategy

The solution of the complete elastic bending problem can be built by a two step procedure:

1. first, a membrane solution is established according to Section 4.1, for which the normal displacement u_n may be incompatible in some specific points of the shell due to discontinuities associated to the external or internal geometry;
2. secondly, a local bending correction is introduced and computed at each discontinuity in order to restore compatibility everywhere in the shell.

In the following, we illustrate the approach for a single discontinuity. For multiple discontinuities, the same principle can be adopted, but the specific formulas given in the following require that the bending corrections associated to two different discontinuities do not interact with each other; in other words, the distance between the discontinuities must be greater than the penetration length.

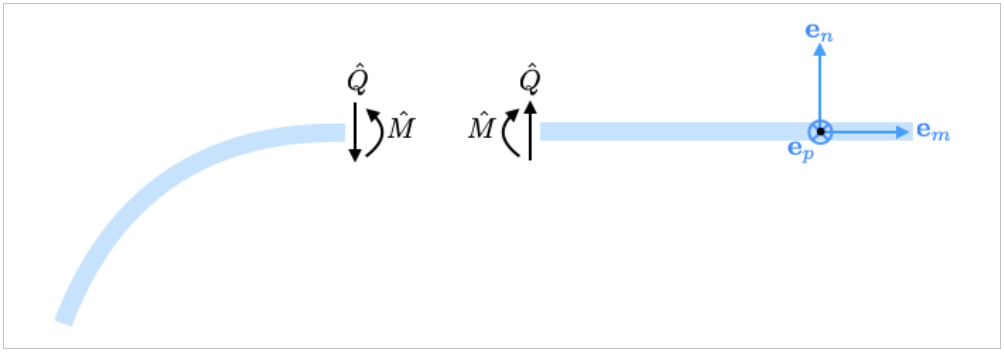

Figure 2: Concentrated loads applied for the bending correction

The bending correction is introduced by applying equal and opposite loads, in the form of a transverse shear force $\hat{Q}$ and a moment $\hat{M}$, on either side of the discontinuity (the positivity convention adopted in the following calculations is given in Figure 2). Any values of $\hat{Q}$ and $\hat{M}$ preserve equilibrium, while an appropriate choice of their values, computed in the following, enables to restore the compatibility of displacements associated to the membrane solution.

Let us set the origin of ξ^m at the discontinuity for convenience. The compatibility condition to restore displacement continuity at $\xi^m = 0$ reads

$$\left(\overbrace{\begin{bmatrix} u_n \\ 0 \end{bmatrix}}^{membrane} + \overbrace{\begin{bmatrix} u_n \\ \phi_m \end{bmatrix}}^{bending} \right) \Bigg|_{\xi^m=0^-} = \left(\overbrace{\begin{bmatrix} u_n \\ 0 \end{bmatrix}}^{membrane} + \overbrace{\begin{bmatrix} u_n \\ \phi_m \end{bmatrix}}^{bending} \right) \Bigg|_{\xi^m=0^+}$$

The membrane displacements are already known from step 1. The bending displacements at the discontinuity can be written as functions of the concentrated loads, as

$$\overbrace{\begin{bmatrix} u_n \\ \phi_m \end{bmatrix} \Big|_{\xi^m=0^i}}^{bending} = \mathbf{S}_i \begin{bmatrix} \hat{Q} \\ \hat{M} \end{bmatrix}$$

where $\mathbf{S}_-$ and $\mathbf{S}_+$ represent the concentrated bending compliance of the two portions of the shell with $\xi^m < 0$ and $\xi^m > 0$, respectively, as seen from the discontinuity. The values of $\hat{Q}$ and $\hat{M}$ can thus be determined by solving the simple system:

$$\overbrace{(\mathbf{S}_- - \mathbf{S}_+) \begin{bmatrix} \hat{Q} \\ \hat{M} \end{bmatrix}}^{bending} + \overbrace{\left(\begin{bmatrix} u_n \\ 0 \end{bmatrix}\Big|_{\xi^m=0^-} - \begin{bmatrix} u_n \\ 0 \end{bmatrix}\Big|_{\xi^m=0^+} \right)}^{membrane} = \mathbf{0} \tag{21}$$

The amplitude of the bending correction terms is thus directly proportional to the mismatch in the membrane displacements. The determination of the matrices $\mathbf{S}_-$ and $\mathbf{S}_+$ is discussed in the following.

As it was stated earlier, the analytical determination of $\mathbf{S}_-$ and $\mathbf{S}_+$ is quite straightforward for a cylindrical shell, but difficult in the general case. Since the bending solution is localized, only the portion of shell in the vicinity of the applied $\hat{Q}$ and $\hat{M}$ plays a role in the determination of the concentrated bending compliance. For this reason, a classical approximation is to replace the matrices $\mathbf{S}_-$ and $\mathbf{S}_+$ for a general shell with the one associated to a cylinder with the same local radius and constitutive behavior [17]: the accuracy of this approximation increases as the bending solution becomes more localized, that is for increasing values of α_1.

The general solution on the bending problem for a cylinder, Eq. (20), can be easily used to determine the analytical expressions of $\mathbf{S}_-$ and $\mathbf{S}_+$. The integration constants $C_1 - C_4$ on either side of the discontinuity can be determined for an applied concentrated force $\hat{Q}$ and moment $\hat{M}$ at $\xi^m = 0$. The displacement and rotation at $\xi^m = 0$ can then be expressed as a function of $\hat{Q}$ and $\hat{M}$, yielding $\mathbf{S}_-$ and $\mathbf{S}_+$. In particular, we have

$$\mathbf{S}_- = \frac{1}{K} \begin{bmatrix} -S_{11} & S_{12} \\ S_{21} & -S_{22} \end{bmatrix}, \quad \mathbf{S}_+ = \frac{1}{K} \begin{bmatrix} S_{11} & S_{12} \\ S_{21} & S_{22} \end{bmatrix}$$

where

$$\begin{aligned} S_{11} &= 2R^3 \tilde{D} \alpha_1 \\ S_{12} &= -R^3 \tilde{B} + R^2 \tilde{D} \left(3\alpha_1^2 - \alpha_2^2\right) \\ S_{21} &= R^3 \tilde{B} + R^2 \tilde{D} \left(\alpha_1^2 + \alpha_2^2\right) \\ S_{22} &= 2R \tilde{D} \alpha_1 \left(\alpha_1^2 + \alpha_2^2\right) \\ K &= R^2 \tilde{B}^2 + 2R \tilde{B} \tilde{D} \left(-\alpha_1^2 + \alpha_2^2\right) + \tilde{D}^2 \left(\alpha_1^2 + \alpha_2^2\right)^2 \end{aligned}$$

Obviously, the terms of the compliance matrices depend on the radius R of the cylinder, as well as on the stiffness terms $\tilde{A}$, $\tilde{B}$ and $\tilde{D}$. These terms are supposed to be constant on each side of the discontinuity, thus this model cannot account for ply reorientation in the dome, or for variations in stiffness which could be associated to progressive degradation. On the other hand, a localized jump in stiffness at the discontinuity, due for example to a ply drop, can easily be taken into account by computing $\mathbf{S}_-$ and $\mathbf{S}_+$ using different stiffness coefficients.

If the coupling is set to zero ($\tilde{B} = 0$, $\alpha_1 = \alpha_2 = \alpha$), the simpler and well-known expressions for balanced laminates and homogeneous shells are recovered.

Once the values of $\hat{Q}$ and $\hat{M}$ which restore the displacement compatibility have been determined from Eq. (21), the numerical values of the coefficients $C1 - C4$ on each side of the discontinuity can be determined as:

- on the left of the discontinuity:

$$C_1 = C_2 = 0, \quad C_3 = \frac{1}{K}\left(K_{11}\hat{Q} - K_{12}\hat{M}\right), \quad C_4 = \frac{1}{K}\left(-K_{21}\hat{Q} + K_{22}\hat{M}\right),$$

- on the right of the discontinuity:

$$C_3 = C_4 = 0, \quad C_1 = \frac{1}{K}\left(K_{11}\hat{Q} + K_{12}\hat{M}\right), \quad C_2 = \frac{1}{K}\left(K_{21}\hat{Q} + K_{22}\hat{M}\right),$$

ou

$$\begin{aligned}
K_{11} &= \frac{1}{\alpha_2}\left(-R^4\tilde{B} + R^3\tilde{D}\left(\alpha_1^2 - \alpha_2^2\right)\right) \\
K_{12} &= \frac{\alpha_1}{\alpha_2}\left(-R^3\tilde{B} + R^2\tilde{D}\left(\alpha_1^2 - 3\alpha_2^2\right)\right) \\
K_{21} &= 2R^3\tilde{D}\alpha_1 \\
K_{22} &= -R^3\tilde{B} + R^2\tilde{D}\left(3\alpha_1^2 - \alpha_2^2\right)
\end{aligned}$$

Using Eq. (20) and the definition of all of the shell quantities as functions of u_n, given in Section 4.2.1, the bending correction can be calculated everywhere in the shell. In particular, knowledge of the membrane and bending strains everywhere in the shell enables one to compute the local stresses in each ply in the material coordinates, in order to detect the most critical points in terms of potential failure locations.

As it was underlined multiple times, the solution resulting from this two steps procedure is still an approximation for multiple reasons:

- the shell theory is only an approximation of the full three-dimensional description;
- in the bending correction, the bending compliances $\mathbf{S}_-$ and $\mathbf{S}_+$ are determined for a cylindrical shell, and not for a general shell;
- in the bending correction, the constitutive behavior was considered constant along the shell, thus not accounting for the evolution of the plies orientation and their eventual degradation.

For this reason, this approach is only suitable for preliminary design, whereas the final design should be validated via two-dimensional axisymmetric or full three-dimensional finite element computation, with a constitutive model which is able to account for the progressive degradation at the scale of the tow.

Table 1: Material properties of the composite tow

E_1 (GPa)	150	E_2 (GPa)	10
G_{12} (GPa)	5	ν_{12} (-)	0.3

5. Some illustrations

The range of material and structural models presented in Sections 3 and 4 can be used to quickly gain insight on the mechanical response of the pressure vessel, and in particular on the role of the different design parameters in determining this response. Some illustrations of these preliminary design steps are given in the following.

All of the examples presented here are run using a pressure vessel constituted of a cylindrical portion of radius $R = 100$ mm, closed by ellipsoidal domes with different ratios between the principal axes. Different stacking sequences are considered, all of which have the total thickness of $t = 12$ mm. This thickness to radius ratio is quite far from the 'thin shells' which are the classical domain of validity of the simplified models discussed here, but it is representative of real ratios for pressure vessels. The simple membrane and bending shell models discussed here are therefore intended only as preliminary design tools, and their results are not expected to be extremely accurate.

The internal loading pressure is taken as $p = 80$ MPa. The material properties of the composite are given in Table 1.

5.1. External geometry

The meridian curve of the ellipsoidal dome is parametrized as follows

$$\mathbf{m}(\xi^m) = R\sin(\xi^m)\mathbf{e}_r + bR\cos(\xi^m)\mathbf{e}_z, \quad 0 \leq \xi^m \leq \pi/2$$

where the dimensionless constant b enables one to choose the ratio between the principal axes. The signed radii of curvature (obtained from the expressions given in the Appendix) are

$$R_m = -\frac{R}{b}\left(\cos^2(\xi^m) + b^2\sin^2(\xi^m)\right)^{\frac{3}{2}}, \quad R_p = -\frac{R}{b}\left(\cos^2(\xi^m) + b^2\sin^2(\xi^m)\right)^{\frac{1}{2}}$$

Obviously, the sphere can be recovered as a special case by setting $b = 1$, which gives $R_m = R_p = -R$.

The meridian curve of the cylinder is parametrized as follows

$$\mathbf{m}(\xi^m) = R\mathbf{e}_r - R\xi^m\mathbf{e}_z, \quad \xi^m \geq 0$$

The signed radii of curvature are:

$$R_m = -\infty, \quad R_p = -R$$

The two portions of the meridian curve are continuous at $z = 0$, but their curvature R_m jumps from a finite value (in the ellipsoid) to infinity in the cylinder. As we will see, this is a source of discontinuity in the membrane stresses, and thus it may engender local bending effects.

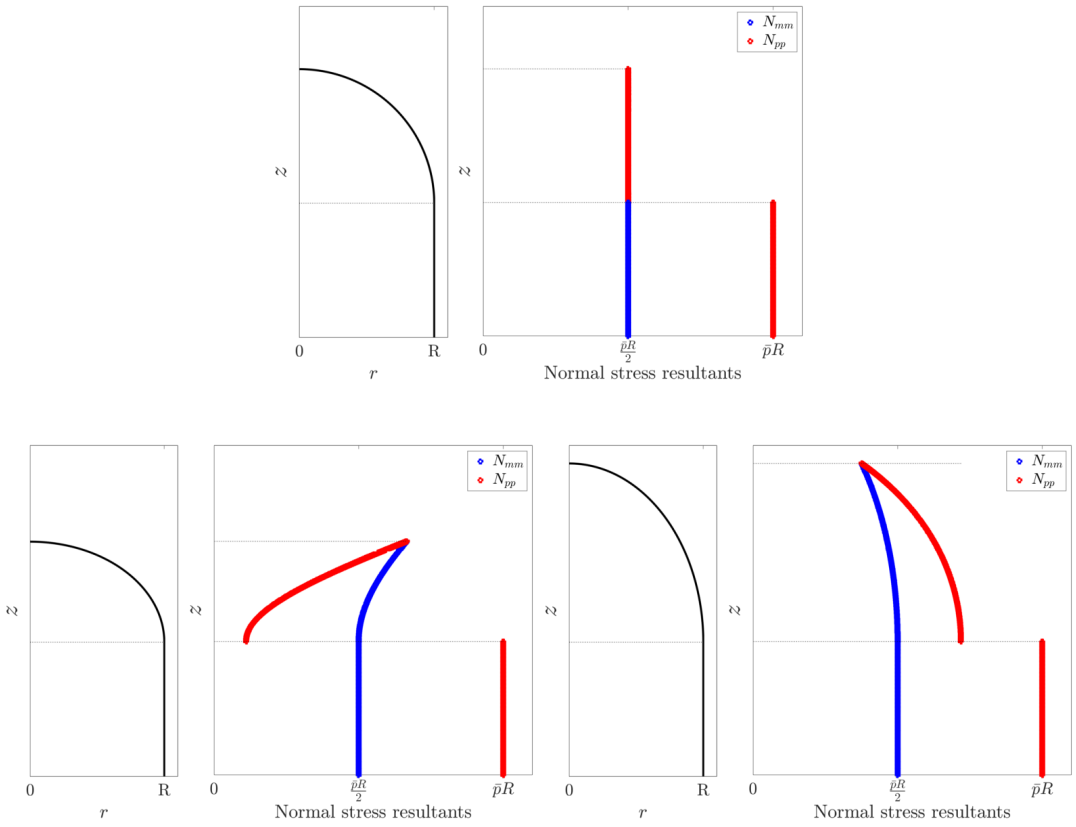

Figure 3: Membrane stresses along z for different dome geometries ($b = 1$, $b = 3/4$ and $b = 4/3$)

5.2. Membrane static analysis

As it was underlined in Section 4.1, the membrane model is isostatic, therefore the membrane stresses $\mathbf{N}$ can be determined independently of the choice of the material model.

Using Eqs. (9) and (10), $\mathbf{N}$ is determined as

- for the ellipsoid

$$\mathbf{N} = \frac{\bar{p}R}{2b}\left(\cos^2(\xi^m) + b^2\sin^2(\xi^m)\right)^{\frac{1}{2}}\left[\begin{array}{ccc} 1 & 2 - \frac{1}{\cos^2(\xi^m)+b^2\sin^2(\xi^m)} & 0 \end{array}\right]^{\mathrm{T}}$$

- for the cylinder

$$\mathbf{N} = \frac{\bar{p}R}{2}\left[\begin{array}{ccc} 1 & 2 & 0 \end{array}\right]^{\mathrm{T}}$$

The values for the cylinder were already introduced in Section 3.1 to discuss optimal orientations and thicknesses determined by netting analysis.

The membrane stresses in the meridian and parallel directions, N_{mm} and N_{pp}, are plotted in Figure 3 for different values of the axes ratio b in the ellipsoid. While in the cylinder the

membrane stresses are constant and $N_{pp} = 2N_{mm}$, their values in the dome are highly dependent on the chosen axes ratio b. For $b < 1$, the radii of curvature, and thus the membrane stresses, are maximum at the dome top ($\xi^m = 0$) and decrease towards the junction with the cylinder ($\xi^m = \pi/2$), while the opposite is true for $b > 1$. For $b = 1$ (spherical dome) the constant curvatures engender equal and constant membrane stress $N_{mm} = N_{pp}$.

While the membrane stress in the meridian direction evolves continuously towards its value $N_{mm} = \frac{\bar{p}R}{2}$ in the cylindrical part, the membrane stress in the parallel direction is always discontinuous at the junction between the dome and the cylinder, due to the discontinuity of the meridian radius of curvature R_m. The discontinuity is greater for smaller values of b, with N_{pp} in the dome eventually becoming compressive (for $b < 1/\sqrt{2}$). Depending on the choice of the stacking sequence, this discontinuity could generate a discontinuity in the membrane strains, and thus the need for a local bending correction, as we will discuss in the next Section.

5.3. Membrane model and netting analysis: optimal orientations and critical points

Here, the netting analysis material model is used to post-treat the results of the membrane structural model. This combination of models is used in the literature for preliminary design of the stacking sequence in the cylinder [5] or to design the optimal dome shape considering only a couple of orientations $\pm\theta$ [18]. Here, we show here that it is particularly useful to anticipate possible critical points in the dome design for any number of orientations $\pm\theta_i$. Furthermore, the interplay between features associated to the external and internal geometry can be used to remove some of these critical points very early in the design process.

The membrane stresses $\mathbf{N}$ being known from the membrane model, the membrane strains $\boldsymbol{\mu}$ can be easily computed from Eq. (13), and the presence of discontinuities in μ_{pp}, which require the introduction of a local bending correction, can be identified. Furthermore, the stresses $\sigma_{11,i}$ for each orientation θ_i can be determined from Eq. (6), thus identifying the position and orientation of the most loaded tows, which will determine the safety factor with respect to bursting in the preliminary design phase.

Three different internal geometries are considered in the following examples. The orientations in the cylindrical portion of the vessel are given as:

1. $[\pm 54.74°]$ in equal proportions;
2. $[\pm 20°, \pm 45°, \pm 70°]$ in the following proportions: $[14, 28, 58] \cdot \frac{t}{100}$;
3. $[\pm 20°, \pm 45°, \pm 70°, 90°]$ in the following proportions: $[22, 22, 22, 33] \cdot \frac{t}{99}$ (where the 90° ply is dropped at the junction).

while their evolution along the dome, computed via Eq. (2), is represented in the left column of Figure 4. At this stage, only the orientations and thicknesses of the different layers are specified: indeed, the stacking sequence, that is the order in which the different orientations and laid on the mandrel, does not modify the response of the purely membrane model. Its role will be investigated later, when the bending correction is considered.

In the cylinder, all three choices are optimal and they have identical total thickness t. In the dome, each orientation evolves according to Clairault's relation (Eq. (2)), dropping

one by one at their respective minimum distances from the axis of revolution (Eq. (3)): in particular, the 90° ply is dropped right at the junction between the cylinder and the dome. The interplay between the external geometry, which determines the membrane stresses $\mathbf{N}$, and the internal geometry, which controls the evolution of the stiffness matrix $\mathbf{A}$, gives rise to complex and sometimes surprising results.

5.3.1. Effect of the internal geometry (orientations and thicknesses)

A spherical dome geometry is considered first. The evolution of the angles, membrane strains and fiber stresses along z for each orientation are plotted in Figure 4 for different internal geometries.

All three of the internal geometries are optimal in the cylinder, thus the stresses in the fibers are all identical in that portion of the pressure vessel. As for the membrane strains μ_{mm} and μ_{pp}, they are identical for cases 2 and 3, while $\mu_{pp} = 2\mu_{mm}$ for case 1.

The situation is significantly different in the dome.

The "famous" optimal solution considered in case 1 has only two orientations, therefore it is not robust with respect to a change in the loading conditions. For this reason, no response can be computed in the dome, in which the membrane stresses $\mathbf{N}$ contain a component which is not included in the image of $\mathbf{A}$. If a fully elastic, rather than a netting, constitutive model was used, the response in the dome would be controlled by the matrix, thus making it much less stiff and prone to failure associated to matrix damage, such as transverse matrix cracking.

The second and third solutions, including more than one couple of orientations, have a much more robust response, at least until the next to last orientation is dropped. After that, they incur in the same problems as described above. The minimum radius at which the next to last orientation is dropped defines the minimum radius of the metal base, which should be present at this point in order to withstand the loads which cannot be carried by the composite.

The membrane strains have complex evolutions along z, in particular in correspondence of geometric accidents and ply drops. For case 2, discontinuities in μ_{pp} occur both at the dome to cylinder junction (due to the discontinuity of N_{pp}) and at the position in which the 70° ply is dropped (leading to the discontinuity of $\mathbf{A}$). Bending corrections should therefore be introduced in both positions, with the ply drop appearing more critical as the jump in strain is higher. For case 3, on the other hand, a single discontinuity at the ply drop is observed. Indeed, at the dome to cylinder junction, two different effects compensate each other:

1. the discontinuity of N_{pp}, generated by the discontinuous curvature (external geometry), which would tend to decrease the strain μ_{pp} in the dome (as it occurs for case 2);
2. the discontinuity of $\mathbf{A}$, generated by dropping the 90° ply (internal geometry), which compensates exactly the first effect, thus finally leading to a continuous μ_{pp} at the junction.

This is a nice example of how the external and internal geometries can be controlled together to remove potentially critical situations.

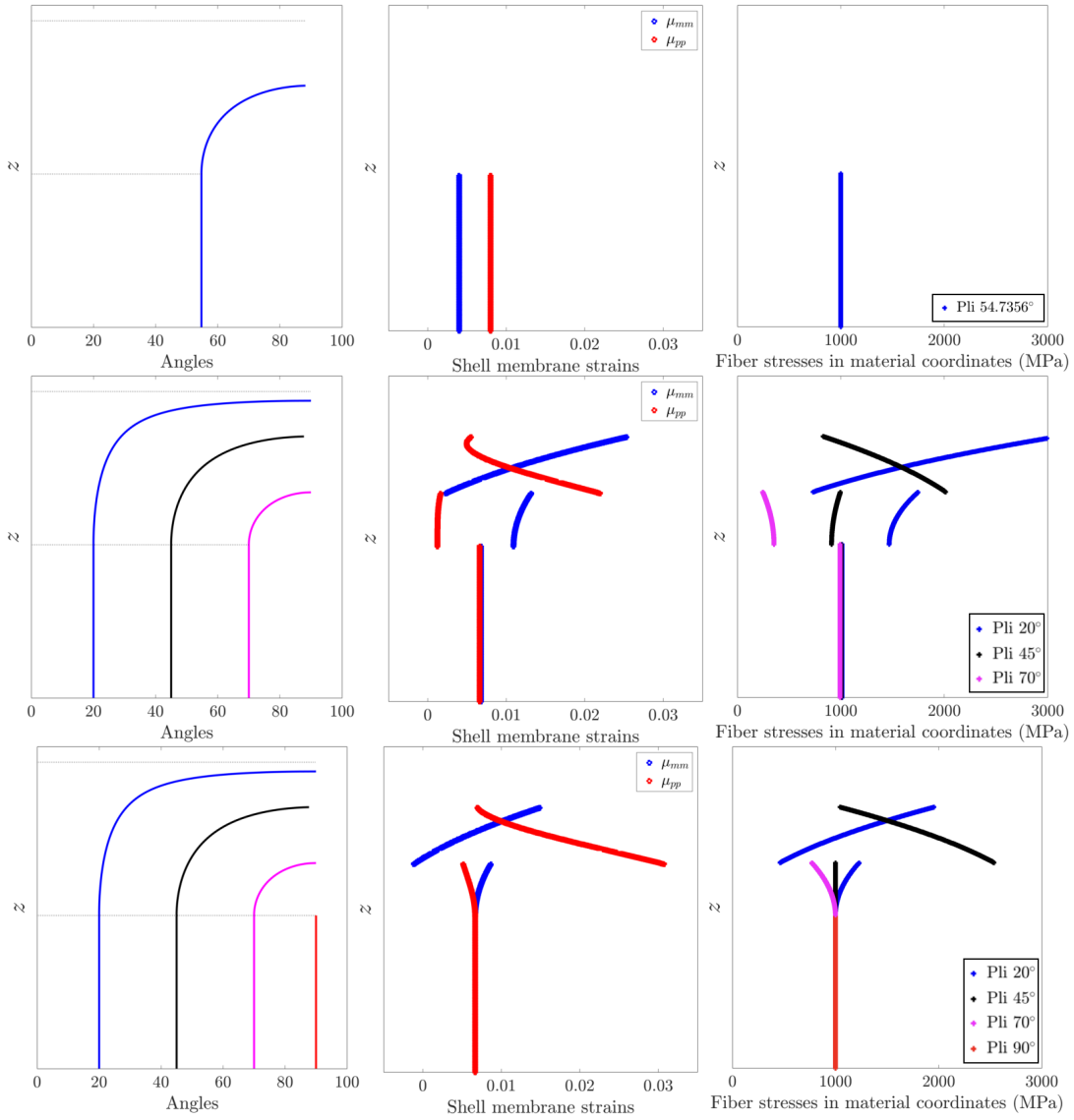

Figure 4: Angles evolution, membrane strains and fiber stresses for different internal geometries, circular dome (membrane model and netting analysis)

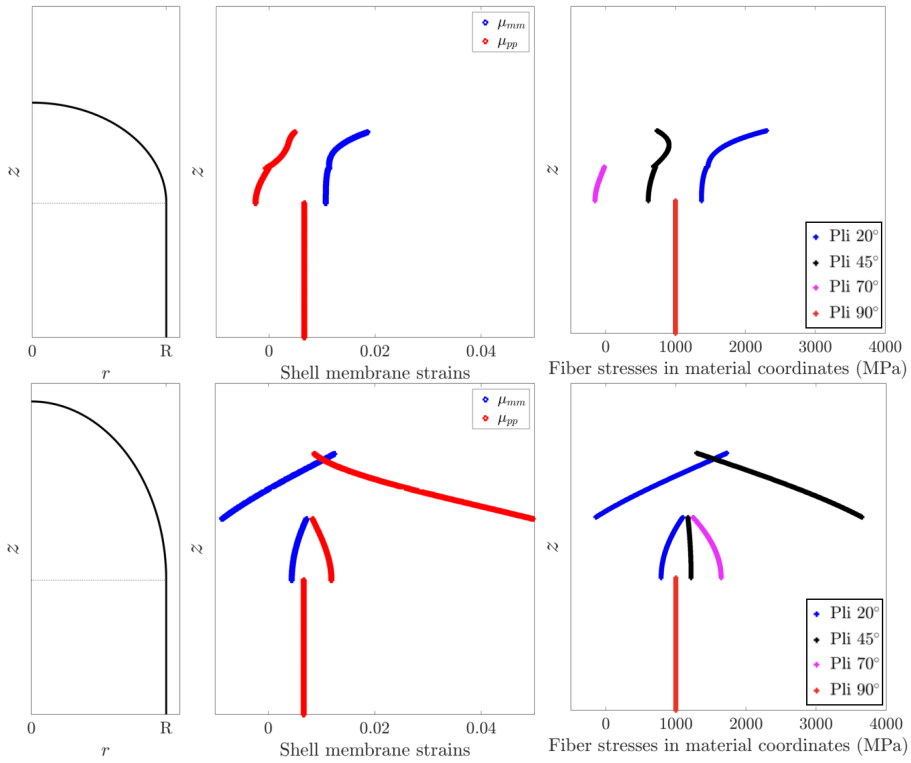

Figure 5: Geometry, membrane strains and fiber stresses for case 3, dome shapes $b = 3/4$ (top figures) and $b = 4/3$ (bottom figures) (membrane model and netting analysis)

The fiber stresses in the different orientations are also significantly different for cases 2 and 3. In both cases, the fibers stresses evolve differently in the different tows, whose orientations change along the dome while the membrane stresses $\mathbf{N}$ stays the same (spherical dome). As it happened for the membrane strains, discontinuities of the fiber stresses occur at the junction and at the 70° ply drop for case 2, and only at the ply drop for case 3. For all three internal geometries, furthermore, the maximum fiber stress always occurs in the dome, and it is significantly higher than the "optimized" value in the cylinder. This confirms the common observation that the dome is indeed the critical zone in composite pressure vessels, and it highlights the importance of this simple tool to anticipate the position and value of the maximum stress due to membrane loadings. A solution to reduce the fiber stresses in the dome without significant oversizing of the cylinder is to add doily layers in specific positions in the dome [5]. This is rather easy to manufacture by laser assisted tape placement in the case of thermoplastic matrix composites.

5.3.2. Effect of the external geometry

The effect of different dome geometries is investigated here for case 3. The dome shape, as well as the evolution of the membrane strains and fiber stresses, are plotted in Figure 5 for two different choices of ellipsoid ($b < 1$ and $b > 1$ respectively).

As it can immediately be noticed, the ellipsoid with $b < 1$ yields lower values of both membrane strains and fiber stresses than the one with $b > 1$. The first geometry is therefore to be preferred. This is coherent with previous findings on the optimal dome shape based on only two orientations [18].

For $b < 1$, indeed, the membrane stress in the meridian direction N_{mm} is higher, but the membrane stress in the parallel direction N_{pp} is lower (and may even become compressive) for a significant portion of the dome height. In particular, it is rather low in correspondence of the 70° ply drop, thus the discontinuity in both membrane strain and fiber stresses in this position nearly disappears. The discontinuity at the junction, on the other hand, re-appears, as the jump in N_{pp} for the ellipsoidal dome is not exactly compensated by 90° ply drop.

This last example (ellipsoidal dome with $b = 3/4$, internal geometry example 3) is used in the following to illustrate the introduction of the bending correction.

5.4. Bending correction and full elastic material model: penetration length and role of the stacking sequence

The first step for the evaluation of the bending terms is the computation of the membrane solution, which enables one to localize and quantify the discontinuities in the displacement, requiring correction. The amplitude of the bending correction is directly proportional to the displacement jump, thus the first approach for limiting the bending response is to design the external and internal geometries in order to optimize as much as possible the membrane response, as it was seen in Section 5.3.

Once the external geometry and the set of tows orientations and thicknesses have been chosen, a last parameter remains in composites design: the stacking sequence. Changing the order in which the different layers are deposited on the mandrel enables the designer a (limited) control over the bending stiffness and the coupling term ($\tilde{D}$ and $\tilde{B}$), while leaving the membrane stiffness ($\tilde{A}$) untouched. As the ratio between membrane and bending stiffness is the main parameter which controls the penetration length, the distance at which the bending effects will be perceived can be partially controlled by appropriate layup choices.

In the following we consider again the example configuration with $b = 3/4$ and the set of orientations and thicknesses associated to case 3. Four different stacking sequences are considered (where the angles are given in the order of deposition on the mandrel):

3.1 $[\pm 20°, \pm 45°, \pm 70°, 90°]$ in the following proportions: $[2, 2, 2, 3] \cdot \frac{t}{9}$;
3.2 $[\pm 90°, \pm 70°, \pm 45°, 20°]$ in the following proportions: $[3, 2, 2, 2] \cdot \frac{t}{9}$;
3.3 $[\pm 20°, \pm 45°, \pm 70°, 90°, \pm 70°, \pm 45°, \pm 20°]$ in the following proportions: $[1, 1, 1, 3, 1, 1, 1] \cdot \frac{t}{9}$;
3.4 $[90°, \pm 70°, \pm 45°, \pm 20°, \pm 45°, \pm 70°, 90°]$ in the following proportions: $[1.5, 1, 1, 2, 1, 1, 1.5] \cdot \frac{t}{9}$.

In all of the cases, the 90° plies are dropped at the junction between the cylinder and the dome.

The results of the complete procedure, membrane solution followed by bending correction, for the four stacking sequences are given in Figures 6 and 7. In particular, Figure 6 gives the minimum and maximum strains in the problem coordinates, while Figure 7 gives the

minimum and maximum fiber stresses for each ply. Indeed, due to the bending component, strains and stresses are no longer constant within each orientation, but they vary linearly between the top and the bottom of each layer. The purely membrane solution, identical for all four sequences, is also reported for completeness: it is slightly different from the one reported in Figure 5, as here the full elastic material behavior was considered. The values of strains and stresses above the next to last ply drop are not taken into consideration, as they are controlled essentially by the matrix response.

Looking at the strain maps (Figure 6) we can notice that the continuity of μ_{pp} was indeed restored at the junction. The strains in the meridian directions, on the other hand, contain both a membrane (μ_{mm}) and a bending (χ_{mm}) component: here, the values at the intrados ($\varepsilon_{mm,b}$) and extrados ($\varepsilon_{mm,t}$) of the cylinder are depicted. As it can be observed, the membrane solution is recovered at some distance from the discontinuity. This distance is not equal in all four cases: in particular, it is obviously longer for case 3, in which the 20° orientations, which contribute most to the bending stiffness $\tilde{D}$ in the meridian direction, are positioned at the greatest distance from the composite midplane. This stacking sequence, therefore, is the worst solution if one wants to limit the penetration length of the bending effects. All of the other cases have similar penetration lengths, of the order of $R/2$. This value is quite high: indeed, as it was pointed out earlier, the shell considered in the examples is far from being a thin shell, with a ratio $t/R = 0.12$. This large penetration length still appears quite reasonable in terms of approximating the involved portion of the dome as the local equivalent cylinder.

The stress maps (Figure 7) are rather complex, as maximum and minimum values for each layer are reported in the same graph. A simplified color code, associated only to the orientation of the layer, was chosen to simplify the reading. Overall, the stresses in the 70° and 90° layers, which are mostly related to the strain μ_{pp}, are rather independent of the stacking sequence, while the layers at 45° and 20° have rather different responses depending on the chosen sequence. Although the most critical stress values are still those computed in the dome for the membrane solution, in an area which is not affected by the junction, some local increases in the fiber stresses with respect to the purely membrane solution can be noticed, particularly in the cylindrical portion of the shell. Again, the worst case scenario seems to be case 3, for which the maximum fiber stress in the cylinder is 20% higher than the one computed with the membrane solution. The other three solutions seem quite similar, with cases 1 and 4 yielding better results for the stresses in the dome. If the critical zones in the dome are resolved with local doily layers or by the presence of the metal base, the overstresses generated by the bending correction may become the critical values for the design of the pressure vessel.

5.5. Comparison with a two-dimensional axisymmetric finite element model

Once a wide range of external and internal geometries have been explored with the membrane model and bending correction, one or two configurations can be retained as a preliminary design and further explored with three-dimensional or two-dimensional axisymmetric finite element models, eventually including the progressive degradation of material properties. Here, the stresses in the fibers direction predicted by the full shell model (membrane

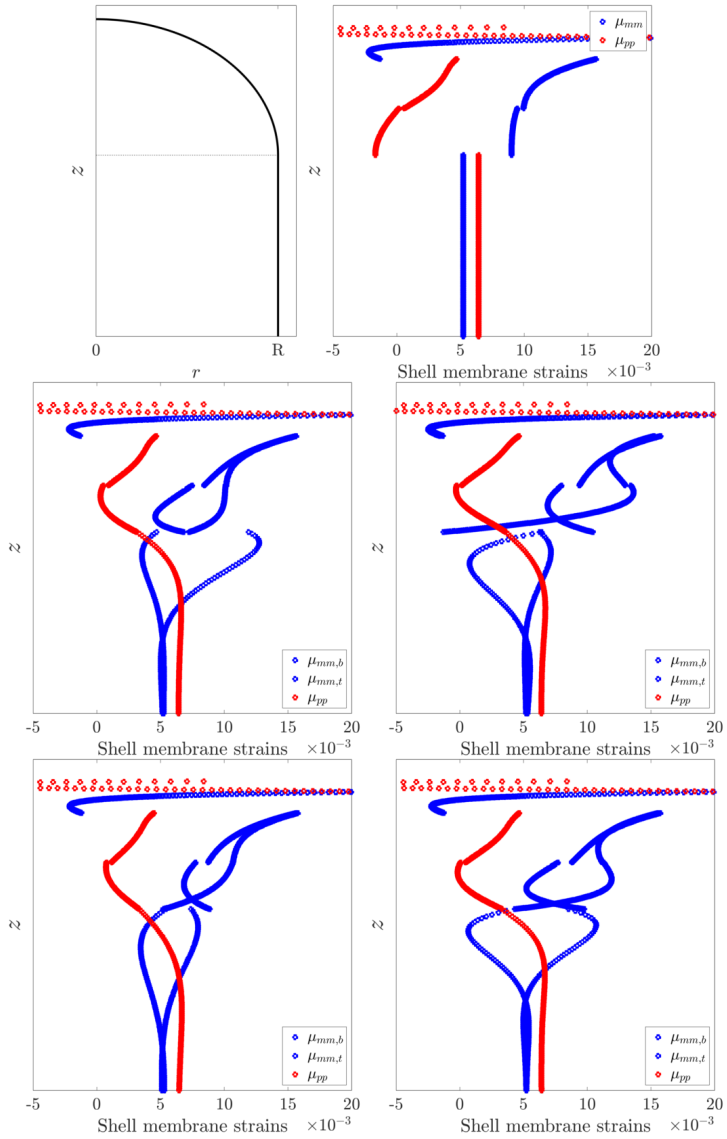

Figure 6: Strains the the problem coordinates for b=3/4, case 3: membrane solution, total solution (membrane and bending correction) for stacking sequences 1 to 4 (full elastic material model)

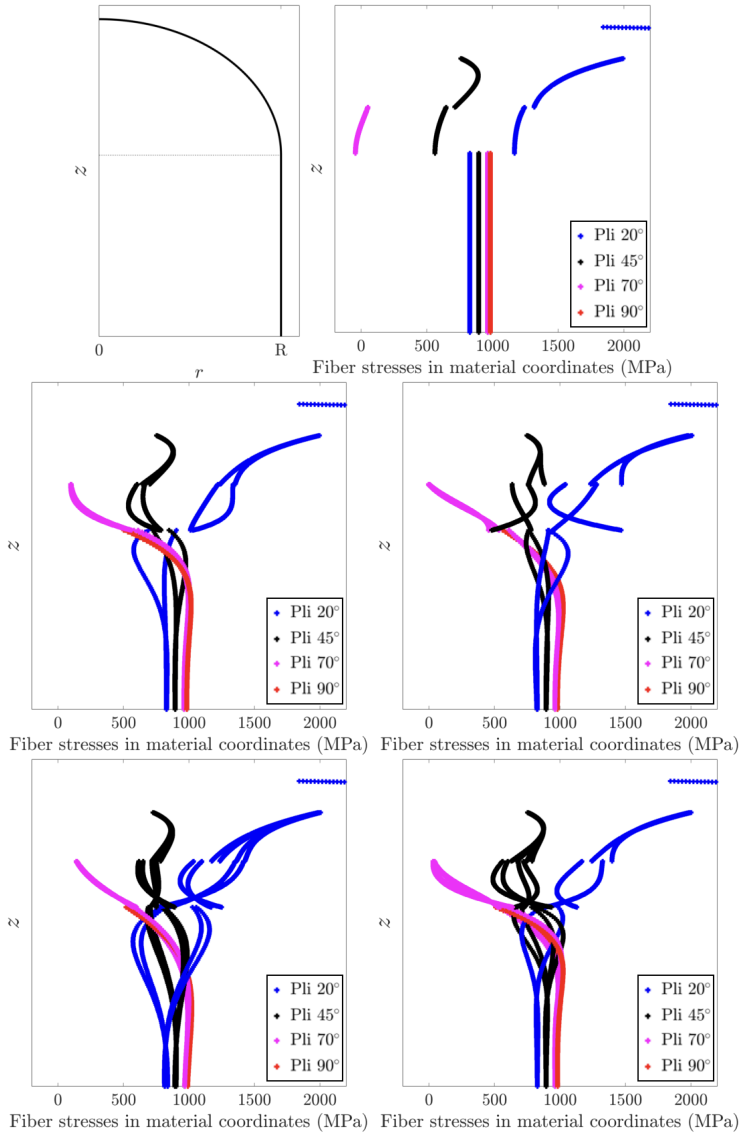

Figure 7: Fiber stresses in the material coordinates for b=3/4, case 3: membrane solution, total solution (membrane and bending correction) for stacking sequences 1 to 4 (full elastic material model)

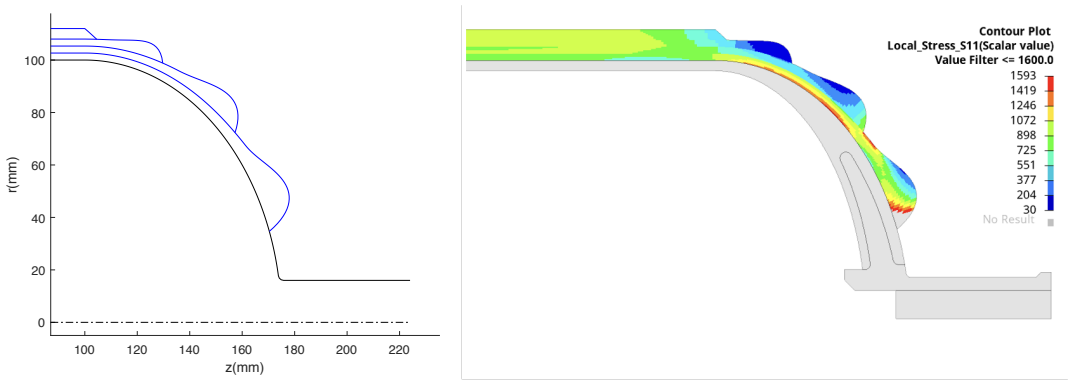

Figure 8: Geometry generated by *OptiTank* (left) and map of the fiber stresses obtained in post-processing (right) for the example illustrated in this work

analysis and bending correction) are compared to those of a linear elastic two-dimensional axisymmetric finite element computation of the pressure vessel provided by Cetim. This enables us to illustrate the following steps of the design process, but also to assess the suitability of the shell model as a preliminary sizing tool.

The model proposed by CETIM is built with an in-house MatLab tool named *OptiTank*. The starting point is a two-dimensional axisymmetric master finite element model, which includes the liner and metallic base geometry and materials, as well as the boundary conditions and loadings. The *OptiTank* tool generates the geometry and material properties of the composite layers, based on a parametric version of the Vasiliev model [24], yielding final geometries in good agreement with the real manufactured parts (see Figure 8, left). The computation is carried out using commercial finite element software (here, Abaqus), then the results are imported back into *OptiTank* for post-processing and visualization in Hyperview (see Figure 8, right).

OptiTank can be used in two differents modes. In the first mode, the user can impose a specific stacking sequence in the cylinder, which is then propagated automatically to the domes. This sequence can be taken as-is, or it can be corrected based on the real tape width to ensure end to end contact of the deposed tapes during manufacturing. In the second mode, the software creates a random set of sequences within a design space to be defined, and the tested sequences are classified according to their mass and mechanical strength.

The major advantage of the *OptiTank* tool is its good performances resulting from automation. Due to its flexible design, additional functionalities can be integrated. One of the outlooks is the evolution of the material laws describing composite. By integrating a damage model as the ones discussed in this work, the *OptiTank* user will be able to simulate the damage and plasticization of the composite for the last iterations of his pressure vessel designs.

The configuration retained here is an ellipsoidal dome with $b = 3/4$, its stacking sequence is number 3.1 from Section 5.4. The whole structure (composite layup, polymer liner, metal base) is accounted for in the finite element model, whereas only the composite layup is

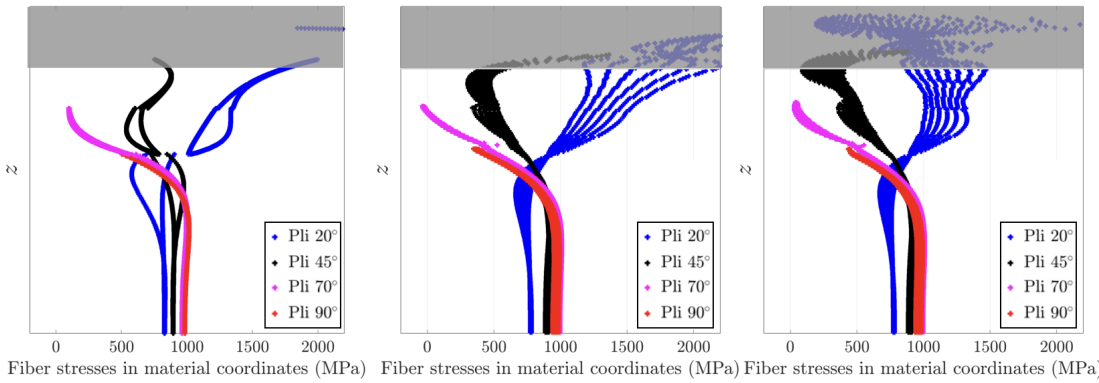

Figure 9: Fiber stresses in the material coordinates for b=3/4, case 3.1: approach proposed here (left) versus two-dimensional axisymmetric finite element computations with constant (center) and variable (right) layer thickness

modeled in the shell description. The external geometry (shell surface) considered for the shell model coincides with the internal surface of the composite (and not with its middle surface): this enables a more accurate evaluation of the overall load seen by the composite, which is given by the pressure p applied over its internal surface.

Two different finite element models were provided by *OptiTank*. In the first, a constant thickness of the composite layers everywhere in the dome is assumed (as in the shell model). In the second (depicted in Figure 8), a more accurate description of the geometry is considered, with the thickness of each composite layer increasing as the local radius decreases.

The results obtained with the different models are displayed in Figure 9. For the shell model, the values at the top and bottom of each ply are plotted as a function of the z coordinate of the shell: these correspond to the maximum and minimum stress seen by each ply. For the axisymmetric finite element models, on the other hand, the stress values are available at the center of each element (Q4 elements with reduced integration), and all of the stress values are plotted as a function of the z coordinate of the element center. Due to the choice of finite element discretization, bending effects might therefore be underestimated by the finite element model.

As it can be observed in the three plots, the values and the evolution of the stresses along z for the different plies are quite similar for the three different models. In particular, the stress values in the central portion of the vessel are well predicted by the simple shell model (the three-dimensional effects are most visible in the 70° and 90° plies, whose fiber stress values are not constant but spread over a interval of a few tens of MPa). The penetration length of the bending effects at the junction is also well predicted by the shell model; the bending effects in the 20° and in the 45° plies seem to be overestimated, but this may be related to the choice of discretization of the finite element model. In the dome, the three models predict very similar stress values until the 70° ply drop (end of the pink line). Above this point, the increase in layer thickness starts to be play a significant role: this effect is visible in the difference between the two finite element models, with the shell model comparing

well to the constant thickness finite element model and overestimating the maximum fiber stresses with respect to the more accurate, variable thickness solution. Finally, the results in the greyed area should not be considered in the comparison: indeed, in this portion of the shell, the metallic base is present in the finite element models and it carries a significant part of the load, which cannot be sustained by the composite layers alone after the 45° ply drop.

Overall, notwithstanding its many approximations, the shell model proposed in this work appears to give good results which can successfully be used for preliminary sizing. Its computational cost is, of course, much lower than its finite element counterpart. The main advantage, however, consists in the clear relationships established between the design choices (external and internal geometry) and the structural response. Such clear understanding and indications for the design are hard, if not impossible, to achieve through a finite element model, even associated to a (cumbersome) parametric study.

6. Conclusions and perspectives

In this work, a hierarchy of material and structural models with increasing levels of detail and complexity is presented and discussed for the design of type IV composite pressure vessels. While most of the models exist in the literature, they were revisited and/or extended here to be used within the overall design strategy. In particular, the membrane solution and bending correction strategy, which was currently used in the past for the design of metal shells of revolution, was extended here to composites with stacking sequences displaying general membrane/bending coupled behavior.

The combination of a simple structural membrane model and a material netting analysis description was extremely useful to understand the crucial role of the shell curvatures and of the orientations and thicknesses of the composite layers in determining the mechanical response of the pressure vessel. In particular, it enabled one to detect and quantify the discontinuities in membrane strains, which give rise to localized bending effects. Furthermore, the interplay between external and internal geometry can be used to remove some of these discontinuities at a very early design stage.

Once these key parameters are fixed, the bending correction can be computed with a full elastic material description. This result is useful to quantify the penetration length of bending effects, which was of the order of the cylinder radius here due to the high thickness to radius ratio. Furthermore, the bending model gives some indications on the best choice of stacking sequence, as the bending effects decrease with decreasing bending stiffness.

The last step of the design strategy consists in a two-dimensional axisymmetric or full three-dimensional computation of the pressure vessel. The use of a material model describing the progressive degradation of the composite material, such as the ones discussed in Section 3.3, constitutes a perspective of this study.

Acknowledgements

This work was funded by Cetim within the framework of the *Laboratoire Commun Comp'Innov*. The PhD scholarship of Duy-Tien Tran was funded by the Doctoral School

SMEMaG (ED 579).

Appendix A. Geometric properties of the surface of revolution

The shape of the pressure vessel is described in this work as a surface of revolution. The placement of the meridian curve in the Euclidean space $\mathbb{R}^3$ was defined in Eq. (1) as

$$\mathbf{m}\left(\xi^m\right) = f_r\left(\xi^m\right)\mathbf{e}_r + f_z\left(\xi^m\right)\mathbf{e}_z$$

The expressions of the geometric properties of interest of the surface of revolution as a function of $f_r(\xi^m)$ and $f_z(\xi^m)$ are reported here.

The metric tensor $\mathbf{g}$ on the surface is expressed as

$$\mathbf{g} = \begin{bmatrix} g_{mm} & 0 \\ 0 & g_{pp} \end{bmatrix} = \begin{bmatrix} f_r'^2 + f_z'^2 & 0 \\ 0 & f_r^2 \end{bmatrix}$$

where the superscript $'$ indicates derivation with respect to the parameter ξ^m.

The local orthonormal basis for the structure, $(\mathbf{e}_m, \mathbf{e}_p, \mathbf{e}_n)$ is expressed as

$$\mathbf{e}_m = \frac{1}{\sqrt{g_{mm}}}\frac{\partial \mathbf{m}}{\partial \xi^m} = \frac{f_r'\mathbf{e}_r + f_z'\mathbf{e}_z}{\sqrt{f_r'^2 + f_z'^2}}, \quad \mathbf{e}_p = \mathbf{e}_\theta, \quad \mathbf{e}_n = \mathbf{e}_m \times \mathbf{e}_p = \frac{-f_z'\mathbf{e}_r + f_r'\mathbf{e}_z}{\sqrt{f_r'^2 + f_z'^2}}$$

The (signed) normal radii of curvature of the surface in the meridian and parallel directions are expressed as

$$R_m = \frac{\left(f_r'^2 + f_z'^2\right)^{\frac{3}{2}}}{-f_r'' f_z' + f_r' f_z''}$$
$$R_p = \frac{f_r\left(f_r'^2 + f_z'^2\right)^{\frac{1}{2}}}{f_z'}$$

The Christoffel symbols are expressed as

$$\Gamma^m_{mm} = \frac{f_r' f_r'' + f_z' f_z''}{f_r'^2 + f_z'^2}$$
$$\Gamma^m_{pp} = \frac{-f_r f_r'}{f_r'^2 + f_z'^2}$$
$$\Gamma^p_{mp} = \Gamma^p_{pm} = \frac{f_r f_r'}{f_r^2}$$

and they are zero for all other permutations of the indexes.

Appendix B. Notations

$\mathbf{A}$	membrane shell stiffness matrix
$\tilde{A}$	modified membrane shell stiffness coefficient
$\mathbf{B}$	membrane/bending shell stiffness matrix
$\tilde{B}$	modified membrane/bending shell stiffness coefficient
c_i	cosine of θ_i
$\mathbf{C}$	stiffness matrix of a layer in the material (layer) basis
$C_1,\ C_2,\ C_3,\ C_4$	integration constants for the bending solution
$\mathbf{D}$	bending shell stiffness matrix
$\tilde{D}$	modified bending shell stiffness coefficient
$(\mathbf{e}_1, \mathbf{e}_2, \mathbf{e}_3)$	unit vectors for the local material (layer) basis
$(\mathbf{e}_m, \mathbf{e}_p, \mathbf{e}_n)$	unit vectors for the local structural (shell) basis
$(\mathbf{e}_r, \mathbf{e}_\theta, \mathbf{e}_z)$	unit vectors for the cylindrical coordinates
$E_1,\ E_2,\ E_3$	Young's moduli in the material directions
$f_r,\ f_z$	scalar functions describing the meridian curve
$\mathbf{g}$	local metric tensor
g	determinant of the metric tensor
$G_{12},\ G_{13},\ G_{23}$	shear moduli in the material directions
$\mathbf{m}$	meridian curve
$\mathbf{M} = [M_{mm},\ M_{pp},\ M_{mp}]^{\mathrm{T}}$	bending moment per unit width in the local structural (shell) basis
$\hat{M}$	moment required to restore continuity of the shell displacement
$\mathbf{N} = [N_{mm},\ N_{pp},\ N_{mp}]^{\mathrm{T}}$	membrane stresses in the local structural (shell) basis
$\mathbf{p} = p\,\mathbf{e}_n$	applied internal pressure
$\mathbf{Q}$	resultant of the applied internal pressure on a portion of the shell
$\hat{Q} = Q_z \mathbf{e}_z$	transverse shear required to restore continuity of the shell displacement
R	radius of the cylindrical portion of the pressure vessel
R_m, R_p	principal (signed) radii of curvature of the meridian and of the parallel
s_i	sine of θ_i
$\mathbf{S}_-,\ \mathbf{S}_+$	concentrated shell bending compliance of the portions with $\xi^m < 0$ and $\xi^m > 0$, respectively, as seen from the discontinuity
t	thickness of the shell
t_i	thickness of the layer i
$\mathbf{T}_i$	rotation operator from the structural (shell) to the material (layer) basis for the layer i
$\mathbf{u}$	shell displacement
$u_m,\ u_n$	components of the shell displacement in the meridian and normal directions
α	parameter related to the penetration length of the bending effects in the uncoupled case
α_1	parameter related to the penetration length of the bending effects in the coupled case
α_2	parameter related to the oscillation of the bending effects in the coupled case
β	corrective parameter related to membrane/bending coupling
Γ^k_{ij}	Christoffel symbols

$\boldsymbol{\varepsilon}_i = \left[\begin{array}{ccc} \varepsilon_{11} & \varepsilon_{22} & 2\varepsilon_{12} \end{array} \right]^{\mathrm{T}}$	strain in the material (layer) basis for the layer i
θ_0	ply orientation in the cylindrical portion of the pressure vessel
θ_i	local ply orientation of layer i
$\boldsymbol{\mu} = [\mu_{mm},\ \mu_{pp},\ \mu_{mp}]^{\mathrm{T}}$	membrane shell strains in the structural (shell) basis
$\nu_{12},\ \nu_{13},\ \nu_{23}$	Poisson's coefficients in the material (layer) directions
ξ^m	parameter of the meridian curve
ξ^n	thickness coordinate of the shell
$\xi^n_i,\ \xi^n_{i+1}$	bottom and top positions in the thickness of layer i
$\boldsymbol{\sigma}_i = \left[\begin{array}{ccc} \sigma_{11} & \sigma_{22} & \sigma_{12} \end{array} \right]^{\mathrm{T}}$	stress in the material (layer) basis for the layer i
ϕ	corrective parameter related to the membrane/bending coupling
ϕ_m	rotation around the $\mathbf{e}_p$ axis of the shell
$\boldsymbol{\chi} = [\chi_{mm},\ \chi_{pp},\ \chi_{mp}]^{\mathrm{T}}$	bending shell strains in the local structural basis
$\bullet'$	derivative of $\bullet$ with respect to the parameter ξ^m

Data availability

The data required to reproduce these findings are available to download from *link to be given when submission is accepted.*

References

[1] ISO11119-1. Gas cylinders - Refillable composite gas cylinders and tubes - Design, construction and testing. Part 1: Hoop wrapped fibre reinforced composite gas cylinders and tubes up to 450L, 2012.

[2] ISO-11119-2. Gas cylinders - Refillable composite gas cylinders and tubes - Design, construction and testing. Part 2: Fully wrapped fibre reinforced composite gas cylinders and tubes up to 450L with load-sharing metal liners, 2012.

[3] ISO-11119-3. Gas cylinders - Refillable composite gas cylinders and tubes. Part 3: Fully wrapped fibre reinforced composite gas cylinders and tubes up to 450L with non-load-sharing metallic or non-metallic liners, 2013.

[4] H. Laeuffer. *Caractérisation et modélisation des réseaux de fissures pour la prédiction de la perméabilité des réservoirs composites stratifiés sans liner.* PhD thesis, ENSAM, 2017.

[5] H. S. Roh, T. Q. Hua, and R. K. Ahluwalia. Optimization of carbon fiber usage in type 4 hydrogen storage tanks for fuel cell automobiles. *International Journal of Hydrogen Energy*, 38:12795–12802, 2013.

[6] B. Gentilleau, F. Touchard, and J. C. Grandidier. Numerical study of influence of temperature and matrix cracking on type IV hydrogen high pressure storage vessel behavior. *Composite Structures*, 111:98–110, 2014.

[7] *Composites Materials Handbook - Volume 3. Polymer matrix composites materials usage, design, and analysis*. Department of Defense Handbook, 2002.

[8] G. Verchery. The netting analysis as a limit case of the laminated structure theory. In *Proceedings of the International Conference on Composite Materials (ICCM-19), Montréal, Canada, 28 July-2 August 2013*, page 1724, 2013.

[9] M. J. Hinton and P. D. Soden. Predicting failure in composite laminates: the background to the exercise. *Composites Science and Technology*, 58:1001–1010, 1998.

[10] M. J. Hinton and A. S. Kaddour. The background to the Second World-Wide Failure Exercise. *Journal of Composite Materials*, 46(19-20):2283–2294, 2012.

[11] A. S. Kaddour, M. J. Hinton, P. A. Smith, and S. Li. The background to the Third World-Wide Failure Exercise. *Journal of Composite Materials*, 47(20-21):2417–2426, 2013.

[12] E. Abisset, F. Daghia, and P. Ladevèze. On the validation of a damage mesomodel for laminated composites by means of open-hole tensile tests on quasi-isotropic laminates. *Composites: Part A*, 42:1515–1524, 2011.

[13] F. Daghia and P. Ladevèze. Identification and validation of an enhanced mesomodel for laminated composites within the WWFE-III. *Journal of Composite Materials*, 47(20-21):2675–2693, 2013.

[14] V. V. Vasiliev and E. V. Morozov. *Mechanics and analysis of composite materials*, chapter Optimal composite structures. Elsevier, 2001.

[15] D. Violeau, P. Ladevèze, and G. Lubineau. Micromodel-based simulations for laminated composites. *Composites Science and Technology*, 69(9):1364–1371, 2009.

[16] P. Ladevèze and E. Le Dantec. Damage modelling of the elementary ply for laminated composites. *Composites Science and Technology*, 43(3):257–267, 1992.

[17] E. H. Baker, A. P. Cappelli, L. Kovalevsky, F. L. Rish, and R. M. Verette. Shell analysis manual. Technical Report NASA-CR-912, NASA, 1968.

[18] M. Hojjati, V. Safavi Ardebili, and S. V. Hoa. Design of domes for polymeric composite pressure vessels. *Composites Engineering*, 5(1):51–59, 1995.

[19] N. J. Pagano and J. M. Whitney. Geometric design of composite cylindrical characterization specimens. *Journal of Composite Materials*, 4:360–378, 1970.

[20] A. A. Vicario and R. R. Rizzo. Effect of length on laminated thin tubes under combined loading. *Journal of Composite Materials*, 4:273–277, 1970.

[21] Olivier Allix, Emmanuel Baranger, and L Blanchard. An efficient strategy for the calculation of end effects on composite pipes: the thermoelastic case. *Composite structures*, 76(4):291–302, 2006.

[22] E Baranger, O Allix, and L Blanchard. A dedicated fourier analysis for the simulation of composite pipes with defects. *International journal for numerical methods in engineering*, 71(1):81–101, 2007.

[23] Emmanuel Baranger, Olivier Allix, and Laurent Blanchard. A computational strategy for the analysis of damage in composite pipes. *Composites Science and Technology*, 69(1):88–92, 2009.

[24] V. V. Vasiliev. *Composite Pressure Vessels: Design, Analysis and Manufacturing*. Bull Ridge Publishing, 2009.